Supplementary Information

for

Multi-Purpose Heterogeneous Catalyst Material from an Amorphous Cobalt Metal–Organic Framework

Kefeng Ping,[‡a] Mahboob Alam,[‡a] Sean Ray Kahnert,[§a] Rohit Bhadoria,[a] Arvo Mere,[b] Valdek Mikli,[b] Maike Käärik,[c] Jaan Aruväli,[d] Päärn Paiste,[d] Arvo Kikas,[e] Vambola Kisand,[e] Ivar Järving,[a] Jaan Leis,[c] Nadežda Kongi[*c] and Pavel Starkov[*a]

[a]Department of Chemistry and Biotechnology, Tallinn University of Technology, Tallinn 12618, Estonia
[b]Department of Materials and Environmental Technology, Tallinn University of Technology, Tallinn 19086, Estonia
[c]Institute of Chemistry, University of Tartu, Tartu 50411, Estonia
[d]Institute of Ecology and Earth Sciences, University of Tartu, Tartu 50411, Estonia
[e]Institute of Physics, University of Tartu, Tartu 50411, Estonia
[‡] K. P. and M. A. contributed equally
[§]Present Address: Clausthal University of Technology, Institute of Organic Chemistry, Leibnizstrasse 6, 38678 Clausthal–Zellerfeld, Germany

**Corresponding authors:*
nadezda.kongi@ut.ee; pavel.starkov@taltech.ee

Table of Contents

1 General

All chemicals were used as supplied. THF was dried over sodium with benzophenone as indicator and distilled. Chromatographic separations were performed on ThoMar OHG silica gel 60Å (40–63 μm). Thin-layer chromatography was performed on Merck TLC Silica gel 60 F_{254} and visualized by UV (254 nm), $KMnO_4$ and/or phosphomolybdic acid. ^1H, ^{19}F and ^{13}C NMR spectra were recorded on Bruker Avance 400 spectrometer. Residual solvent peaks were used as internal standards [1]. Chemical shifts are quoted in ppm using the following abbreviations: s, singlet; d, doublet; t, triplet; qt, quartet; p, pentet; m, multiplet; or a combination thereof.

2 Preparation of TAL-2 catalyst materials

Synthesis of TAL–2. $CoCl_2 \cdot 6H_2O$ (3.96 g, 16.64 mmol, 1.0 equiv) was added dropwise into a mixture of 1*H*-benzo[*d*]imidazole-5,6-diol (5.00 g, 33.30 mmol, 2.0 equiv) in 25% aq. NH_3/DMF/EtOH/water (4:10:10:15), the resulting solution was left to stir at RT. After 24 h, it was filtered, washed with EtOH and dried to give the desired material as a dark green solid (6.28 g).

Synthesis of TAL–2 derived catalyst materials. TAL–2 was carbonized at optimized temperature of 800, 900 or 1000 °C under N_2 for 2 h (rapid heat, rapid cooling). Carbonized materials were suspended in 0.5 M HNO_3, stirred for 8 h at 50 °C, filtered, and recarbonized under N_2 at the same temperature (2 h) to give final catalyst materials. The resulting powders are designated as TAL–2–800, TAL–2–900 and TAL–2–1000.

3 Morphological and physical characterization

HRTEM. TEM measurements were performed using a JEOL-2200FS FEG (S)TEM equipped with Schottky field emission gun (FEG) and operating at accelerating voltage of 200 kV [2]. TEM samples were dispersed in 2-propanol and sonicated for 10 minutes. The resulted suspension was pipetted on a 200 mesh copper grid covered by carbon film.

SEM. Scanning electron microscopy (SEM) measurements were performed using Zeiss Ultra–55. Sample powder was deposited onto the carbon tape. In order to improve the conductivity of initial TAL–2 sample, it was covered with a thin gold layer.

XPS. XPS measurements were performed by SCENTA SES-100 spectrometer equipped with a 300 W non-monochromatic Mg K_α X-ray source (incident energy = 1253.6 eV) and electron take-off angle 90º. During XPS spectra collection, analysis chamber pressure was below 10^{-9} Torr. For collecting survey spectra and high-resolution XPS spectra step sizes of 0.5 eV and 0.1 eV were used, respectively. Pass energy was 200 eV in both cases. XPS sample was prepared by coating GC plate with catalyst suspension in 2-propanol. For fitting of peaks in high-resolution N1s, C1s and Co2p spetra, CasaXPS (2.3.18) software was used.

XRD. The XRD patterns for the TAL-2 samples were recorded on a Bruker D8 Advance diffractometer using Ni filtered Cu K_α radiation and LynxEye line detector. Scanning steps were 0.013º 2θ from 5º to 90º, 2θ and total counting time was 173 s/step. The scan axes were $2\theta/\theta$.

Nitrogen physisorption. Before measurements, the samples were dried for 12 h in vacuum at 150 °C. Low-temperature nitrogen adsorption was done at the boiling temperature of nitrogen (77 K) by using the NOVAtouch LX2 (Quantachrome Instruments). Specific surface area (Sa_{BET}) of carbon samples was calculated from N_2 adsorption corresponding to the BET theory [3] in the P/P_0 interval of 0.02–0.2, the total pore volume (V_{tot}) was calculated at P/P_0 of 0.97. The calculations of pore size distribution (PSD) and specific surface area (Sa_{dft}) from N_2 isotherms were done by using a quenched solid density functional theory (QSDFT) equilibria model for slit type pores. All calculations were done using TouchWin 1.11 software (Quantachrome Instruments).

MP–AES. The samples were dissolved with Anton Par Multiwave PRO microwave digestion system using NXF100 digestion vessels (PTFE–TFM liner) in 8 N rotor prior to analysis. 10 mg of sample was weighed into PTFE vessels into which 4 ml of 69 % HNO_3 (Carl Roth ROTIPURAN Supra) and 2 ml of H_2O_2 (Sigma–Aldrich TraceSelect) were sequentially and slowly added. After the initial reaction had subsided the vessels were capped and digested in the microwave unit at 240 °C and 45–50 bar pressure. After digestion, the samples were diluted using 2 % HNO_3 (prepared from 69 % HNO_3) to final concentration of around 4 mg/L and analyzed using Agilent MP–AES 4210. Cobalt was measured at Co 340.512 nm.

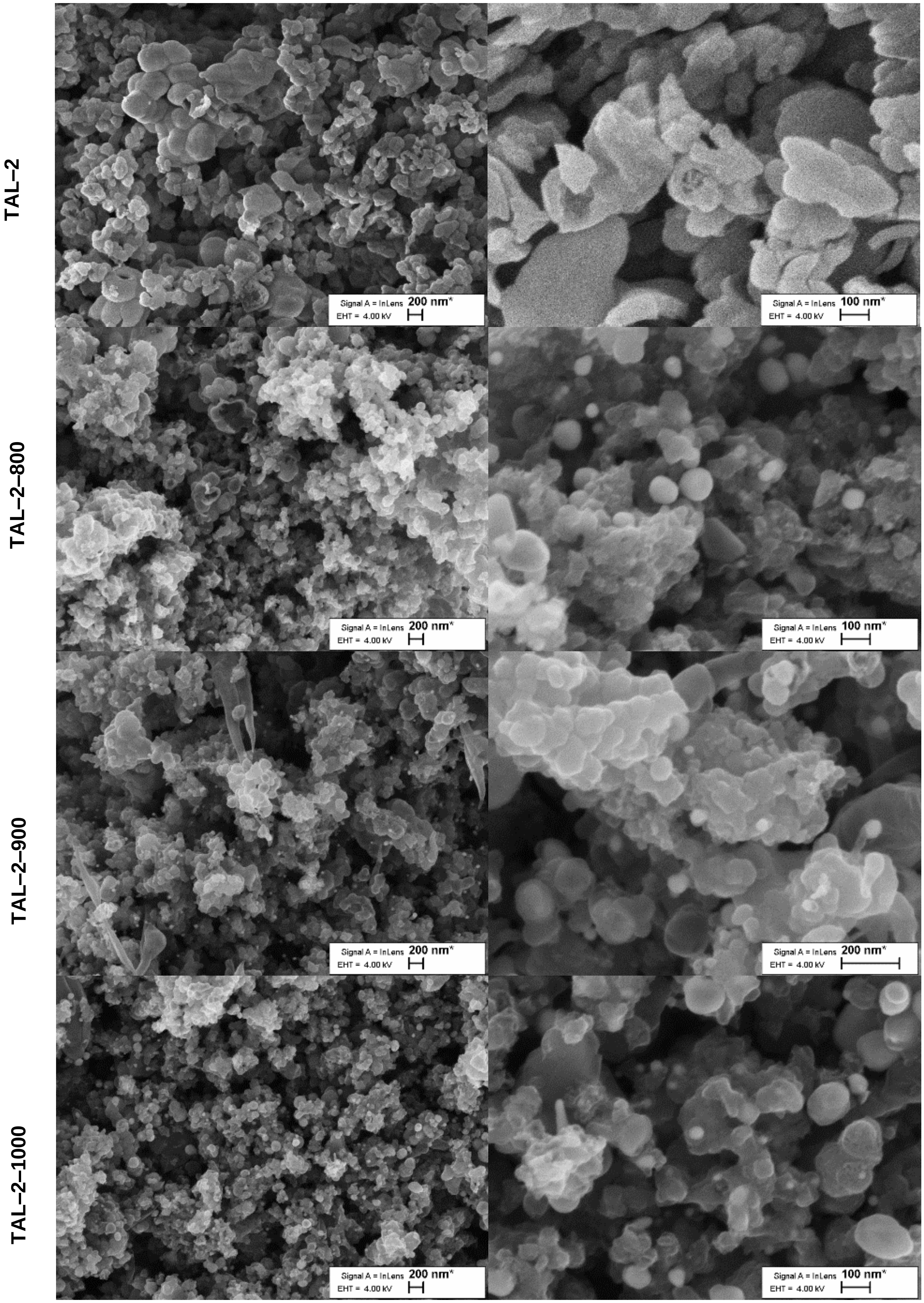

Figure S1. SEM micrographs of TAL–2, TAL–2–800, TAL–2–900 and TAL–2–1000.

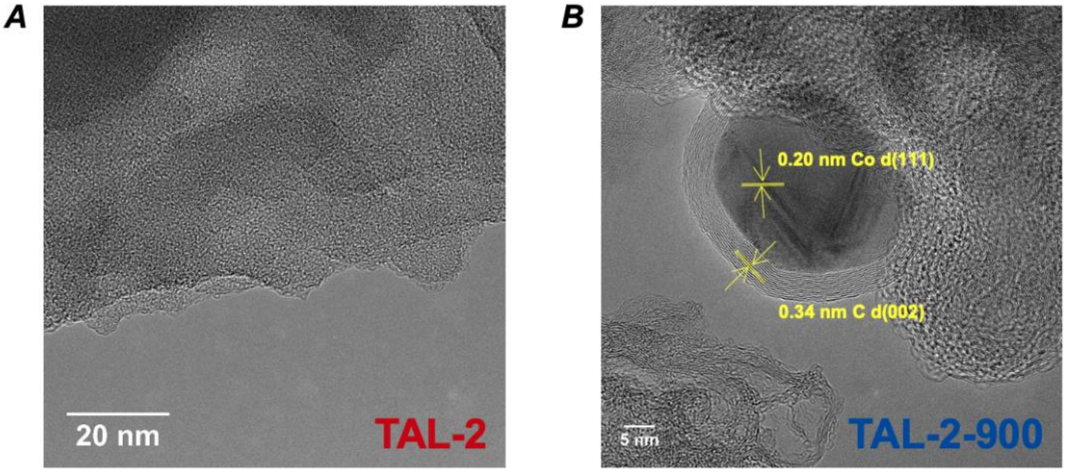

Figure S2. HRTEM micrographs of amorphous MOF TAL–2 and TAL–2–900.

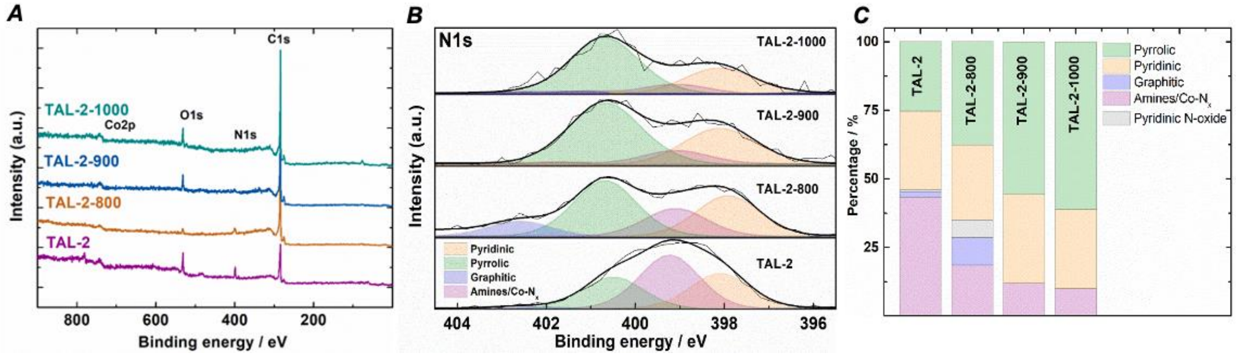

Figure S3. (A) XPS survey spectra. (B) XPS core-level spectra in the N1s region. (C) Distribution of various nitrogen species in the N1S region.

Table S1. Elemental composition of the TAL–2 derived materials' surface by XPS (at%). Total cobalt content by MP–AES (wt%).

material	XPS				MP-AES
	C at%	N at%	O at%	Co at%	Co wt%
TAL-2	75.8	11.5	11.3	1.40	18.003 ± 0.131
TAL-2-800	93.1	4.6	2.1	0.19	5.453 ± 0.029
TAL-2-900	93.5	1.5	4.9	0.13	23.606 ± 0.142
TAL-2-1000	93.0	0.8	6.1	0.14	20.981 ± 0.262

Table S2. Distribution of various nitrogen species at the surface of the catalysts.

material	graphitic N %	N-oxide %	pyridinic N %	amines/Co–N$_x$ %	pyrrolic N %
TAL-2	2.1	0.5	28.8	43.4	25.3
TAL-2-800	10.1	6.5	27.3	18.6	37.6
TAL-2-900	0.0	0.0	32.6	11.9	55.5
TAL-2-1000	0.0	0.0	28.9	10.1	61.0

Table S3. Distribution of various carbon species at the surface of the catalysts.

material	C–O–C, C–OH %	C=O %	O–C=O %	carbide %	π–π* %	sp^2 %	sp^3 %
TAL-2	19.8	10.5	1.1	3.3	1.4	25.8	38.1
TAL-2-800	6.6	4.3	1.9	4.6	5.9	60.3	16.4
TAL-2-900	6.8	4.0	2.0	5.0	6.0	61.5	14.6
TAL-2-1000	5.9	3.2	0.2	5.5	8.1	65.1	12.0

Table S4. Distribution of various oxygen species at the surface of the catalysts.

material	Co oxide %	carbonyl, (ArOH) %	ether %	noncarbonyl, phenols %	quinones %	water %
TAL-2	6.4	30.8	9.8	13.0	40.0	0.0
TAL-2-800	19.6	26.3	19.3	18.6	13.9	2.2
TAL-2-900	5.3	30.8	27.7	8.3	26.8	1.0
TAL-2-1000	9.1	48.3	4.0	10.2	27.6	0.8

Table S5. Distribution of various cobalt species at the surface of the catalysts.

material	Co(0) %	P1-Co(OH)$_2$ %	P2-Co(OH)$_3$ %	P3-Co(OH)$_2$_sattelite %
TAL-2	0.1	33.5	23.4	43.1
TAL-2-800	2.5	35.8	25.1	36.6
TAL-2-900	4.3	28.5	20.0	47.3
TAL-2-1000	4.4	15.3	10.7	69.7

4 Oxidative transformations

Table S6. Recyclability of TAL–X derived catalysts in oxidation of toluene into benzoic acid.[a]

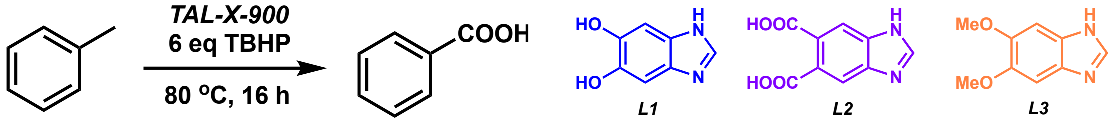

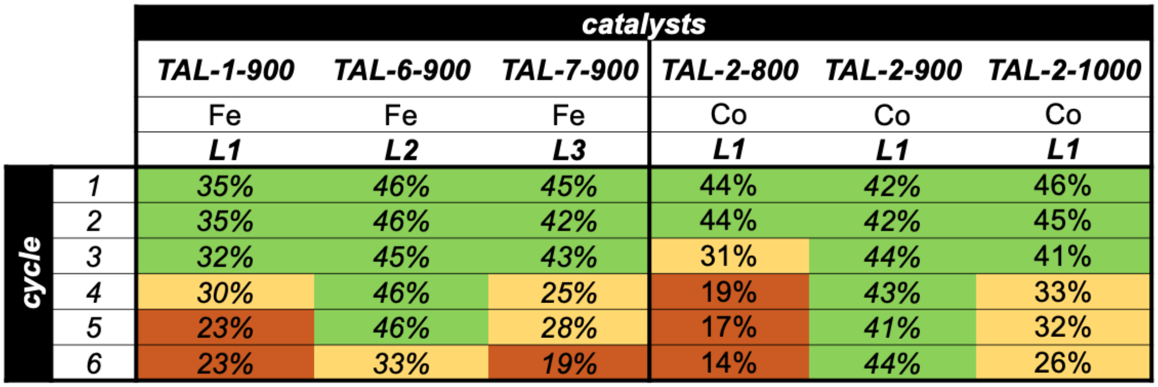

		catalysts					
		TAL-1-900	***TAL-6-900***	***TAL-7-900***	***TAL-2-800***	***TAL-2-900***	***TAL-2-1000***
		Fe	Fe	Fe	Co	Co	Co
		L1	***L2***	***L3***	***L1***	***L1***	***L1***
cycle	*1*	*35%*	*46%*	*45%*	44%	*42%*	46%
	2	*35%*	*46%*	*42%*	44%	*42%*	45%
	3	*32%*	*45%*	*43%*	31%	*44%*	41%
	4	*30%*	*46%*	*25%*	19%	*43%*	33%
	5	*23%*	*46%*	*28%*	17%	*41%*	32%
	6	*23%*	*33%*	*19%*	14%	*44%*	26%

[a] Reaction conditions: toluene (100 mg), TAL–2–900 (5.4 mg), 6 eq TBHP (892 µL), 80 °C, 16 h

[b] NMR yield with 1,3,5-trimethoxybenzene as internal control

Table S7. Recyclability of TAL–X derived catalysts in oxidation of diphenylmethane into benzophenone.[a]

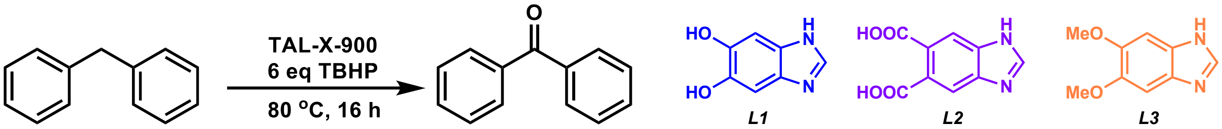

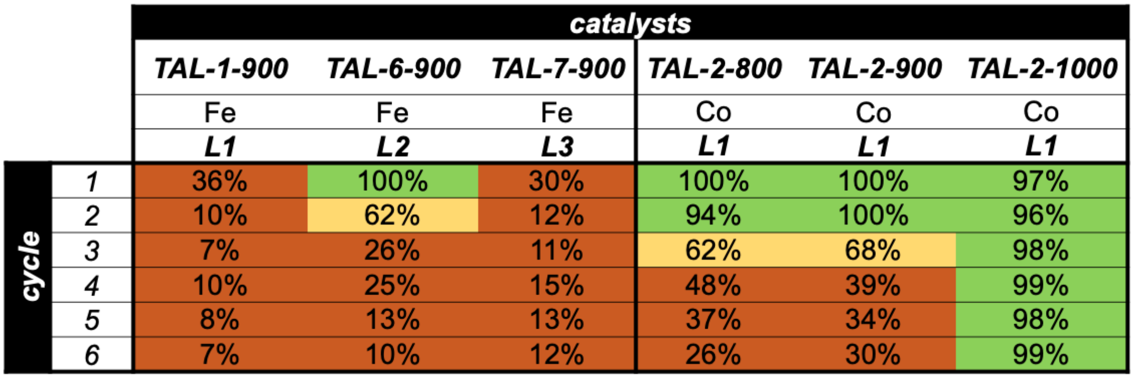

		catalysts					
		TAL-1-900	***TAL-6-900***	***TAL-7-900***	***TAL-2-800***	***TAL-2-900***	***TAL-2-1000***
		Fe	Fe	Fe	Co	Co	Co
		L1	***L2***	***L3***	***L1***	***L1***	***L1***
cycle	*1*	36%	100%	30%	100%	100%	97%
	2	10%	62%	12%	94%	100%	96%
	3	7%	26%	11%	62%	68%	98%
	4	10%	25%	15%	48%	39%	99%
	5	8%	13%	13%	37%	34%	98%
	6	7%	10%	12%	26%	30%	99%

[a] Reaction conditions: diphenylmethane (150 mg), TAL–2–900 (4.5 mg), 6 eq TBHP (732 µL), 80 °C, 16 h

[b] NMR yield with 1,3,5-trimethoxybenzene as internal control

Table S8. Effect of additive in the oxidation of toluene to benzoic acid.[a]

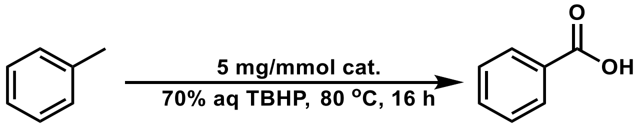

entry	additive	equiv	yield[b]
1	–	–	42%
2[c]	–	–	0
3	TsOH	0.2	20%
4	AcOH	0.1	46%
5	AcOH	0.5	45%
6	***AcOH***	***1.0***	***56%***
7	***AcOH***	***2.0***	***62%***
8	***AcOH***	***3.0***	***60%***
9[c]	AcOH	1.0	0%
10	AcOH+ $B(OMe)_3$	1.0	41%
11	$B(OMe)_3$	1.0	43%
12[d]	AcOH	1.0	33%
13	TFA	0.1	25%
14	TFA	0.5	26%
15	TFA	1.0	17%
16	TFA	2.0	11%
17	TFA	3.0	4%
18	TCA	1.0	28%
19	benzoic acid	1.0	46%
20	Et_3N	0.1	34%
21	Et_3N	0.2	34%
22	Et_3N	0.5	34%
23	Et_3N	1.0	29%
24	pyridine	1.0	21%

[a] Reaction conditions: toluene (100 mg), TAL–2–900 (5.4 mg), 6 eq TBHP (892 µL), 80 °C, 16 h
[b] NMR yield with 1,3,5-trimethoxybenzene as internal control
[c] 6 equiv of H_2O_2 as oxidant
[d] MeCN (2 mL) as solvent

$$\mathbf{PhCH_3}\quad \textit{or}\quad \mathbf{PhCH_2OH}\quad \textit{or}\quad \mathbf{PhCH_2COOH}\ \xrightarrow[\text{70\% aq TBHP, 80 °C, 24 h}]{\text{5 mg/mmol cat.}}\ \mathbf{PhCOOH}$$

From toluene. A mixture of toluene (100 mg, 1.08 mmol, 1.0 equiv), 70% TBHP (892 µL, 6.48 mmol, 6.0 equiv) and TAL–2–900 (5.4 mg) was left to stir at 80 °C. After 24 h, it was filtered through a Celite pad using MeOH, concentrated under reduced pressure, the residue was redissolved in K_2CO_3 solution (10 mL), washed with DCM (2×10 mL), the combined aqueous phase was acidified with HCl, extracted with DCM (3×10 mL), dried over $MgSO_4$ and concentrated under reduced pressure to give the desired product as a colorless solid (59.7, 0.489 mmol, 45%).

From benzylalcohol. A mixture of benzyl alcohol (100 mg, 0.925 mmol, 1.0 equiv), 70% TBHP (760 µL, 5.54 mmol, 6.0 equiv) and TAL–2–900 (4.6 mg) was left to stir at 80 °C. After 24 h, it was filtered through a Celite pad using MeOH, concentrated under reduced pressure, the residue was redissolved in K_2CO_3 solution (10 mL), washed with DCM (2×10 mL), the combined aqueous phase was acidified with HCl, extracted with DCM (3×10 mL), dried over $MgSO_4$ and concentrated under reduced pressure to give the desired product as a colorless solid (105.2, 0.861 mmol, 93%).

From phenylacetic acid. A mixture of 2-phenylacetic acid (100 mg, 0.734 mmol, 1.0 equiv), 70% TBHP (602 µL, 4.40 mmol, 6.0 equiv) and TAL–2–900 (3.7 mg) was left to stir at 80 °C. After 24 h, it was filtered through a Celite pad using MeOH, concentrated under reduced pressure, purified by flash chromatography (EtOAc/PE 1:20) to give the desired product as a colorless solid (72.2 mg, 0.591 mmol, 81%).

Benzoic acid [4]:

^{1}H NMR (400 MHz, $CDCl_3$) δ 8.13 (d, 2H, *J* = 7.1), 7.63 (t, 1H, *J* = 7.4), 7.49 (t, 2H, *J* = 7.7).

^{13}C NMR (100 MHz, $CDCl_3$) δ 172.5, 134.0, 130.4, 129.4, 128.6.

$$\mathrm{PhCH_2CH_3} \xrightarrow[\text{70\% aq TBHP, 80 °C, 24 h}]{\text{5 mg/mmol cat.}} \mathrm{PhCOCH_3}$$

A mixture of ethylbenzene (100 mg, 0.942 mmol, 1.0 equiv), 70% TBHP (774 µL, 5.66 mmol, 6.0 equiv) and TAL–2–900 (4.7 mg) was left to stir at 80 °C. After 24 h, it was filtered through a Celite pad using MeOH, concentrated under reduced pressure and purified by flash chromatography (EtOAc/PE 1:100) to give the desired compound as a colorless oil (95.0 mg, 0.791 mmol, 84%).

Acetophenone [5]:

^{1}H NMR (400 MHz, $CDCl_3$) δ 7.96–7.93 (m, 2H), 7.57–7.53 (m, 1H), 7.47–7.43 (m, 2H), 2.59 (s, 3H).

^{13}C NMR (100 MHz, $CDCl_3$) δ 198.2, 137.2, 133.2, 128.6, 128.4, 26.7.

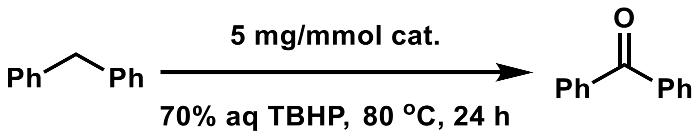

A mixture of diphenylmethane (150 mg, 0.892 mmol, 1.0 equiv), 70% TBHP (732 µL, 5.34 mmol, 6.0 equiv) and TAL–2–900 (4.5 mg) was left to stir at 80 °C. After 24 h, it was filtered through a Celite pad using DCM, and concentrated under reduced pressure to give the desire compound as a colorless solid (157.4 mg, 0.864 mmol, 97%).

^{1}H NMR (400 MHz, $CDCl_3$) δ 7.82–7.79 (m, 4H), 7.61–7.57 (m, 2H), 7.48 (t, 4H, *J* = 7.6).

^{13}C NMR (100 MHz, $CDCl_3$) δ 196.9, 137.7, 132.5, 130.2, 128.4.

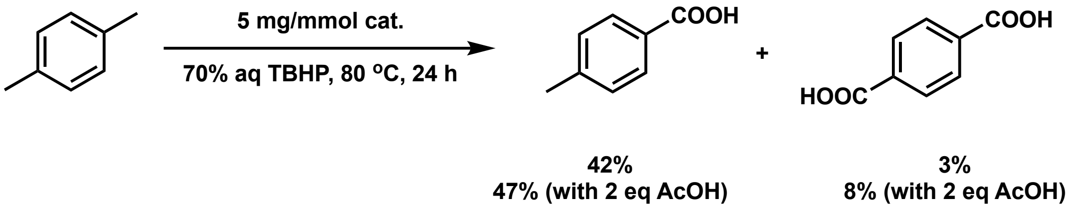

A mixture of *p*-xylene (100 mg, 0.942 mmol, 1.0 equiv), 70% TBHP (1.55 mL, 11.30 mmol, 12.0 equiv) and TAL–2–900 (4.7 mg) was left to stir at 80 °C. After 24 h, it was concentrated under reduced pressure and the residue was purified by flash chromatography (EtOAc/PE 1:20 → 1:10) to give the desired products 4-methylbenzoic acid (53.8 mg, 0.395 mmol, 42%) and terephthalic acid (4.6 mg, 0.028 mmol, 3%), both as colorless solids.

The reaction was repeated in the presence of acetic acid (107.7 µL, 1.884 mmol, 2 equiv) as an additive to give 4-methylbenzoic acid (60.7 mg, 0.446 mmol, 47%) and terephthalic acid (125 mg, 0.075 mmol, 8%).

4-Methylbenzoic acid [6]:

^{1}H NMR (400 MHz, CDCl$_3$) δ 8.01 (d, 2H, *J* = 8.1), 7.28 (d, 2H, *J* = 8.1), 2.43 (s, 3H).

^{13}C NMR (100 MHz, CDCl$_3$) δ 171.9, 144.8, 130.4, 129.4, 126.7, 21.9.

Terephthalic acid [7]:

^{1}H NMR (400 MHz, DMSO–d_6) δ 13.29 (s, 2H), 8.04 (s, 4H).

^{13}C NMR (100 MHz, DMSO–d_6) δ 166.7, 134.5, 129.5.

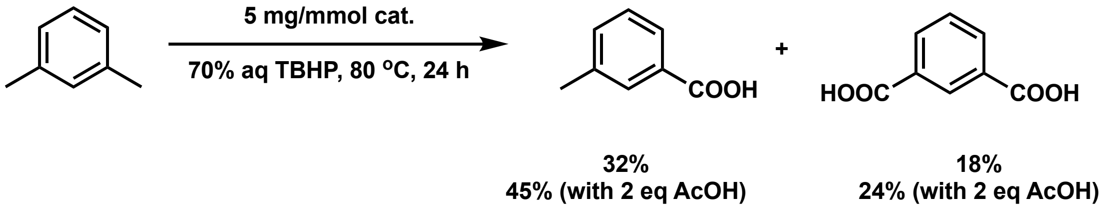

A mixture of *m*-xylene (100 mg, 0.942 mmol, 1.0 equiv), 70% TBHP (1.55 mL, 11.30 mmol, 12.0 equiv) and TAL–2–900 (4.7 mg) was left to stir at 80 °C. After 24 h, it was concentrated under reduced pressure and the residue was purified by flash chromatography (EtOAc/PE 1:20 → 1:10) to give the desired products 3-methylbenzoic acid (40.9 mg, 0.300 mmol, 32%) and isophthalic acid (28.9 mg, 0.174 mmol, 18%) as colorless solid.

The reaction was repeated in the presence of acetic acid (107.7 µL, 1.884 mmol, 2 equiv) as an additive, to give 3-methylbenzoic acid (58.1 mg, 0.427 mmol, 45%) and isophthalic acid (37.3 mg, 0.224 mmol, 24%).

3-Methylbenzoic acid [7]:

^{1}H NMR (400 MHz, DMSO-d_6) δ 12.86 (s, 1H), 7.76–7.73 (m, 2H), 7.43–7.35 (m, 2H), 2.35 (s, 3H).

^{13}C NMR (100 MHz, DMSO-d_6) δ 167.4, 137.9, 133.5, 130.7, 129.8, 128.5, 126.5, 20.8.

Isophthalic acid [8]:

^{1}H NMR (400 MHz, DMSO–d_6) δ 13.2 (s, 2H), 8.48 (s, 1H), 8.17 (d, 1H, J = 1.6), 8.15 (d, 1H, J = 1.6), 7.64 (t, 1H, J = 7.7).

^{13}C NMR (100 MHz, DMSO–d_6) δ 166.6, 133.4, 131.2, 130.0, 129.2.

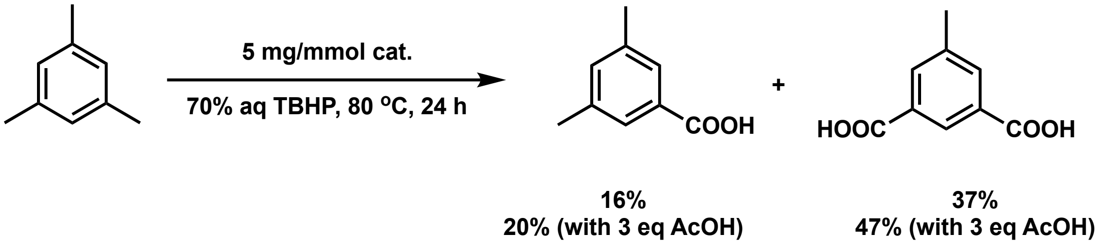

A mixture of mesitylene (100 mg, 0.832 mmol, 1.0 equiv), 70% aq TBHP (2.05 mL, 14.98 mmol, 18.0 equiv) and TAL–2–900 (4.2 mg) was left to stir at 80 °C. After 24 h, it was concentrated under reduced pressure and the residue was purified by flash chromatography (EtOAc/PE 1:20 → 1:10) to give the desired products 3,5-dimethylbenzoic acid (20.5 mg, 0.137 mmol, 16%) and 5-methylisophthalic acid (55.6 mg, 0.309 mmol, 37%) as colorless solids.

The reaction was repeated in the presence of acetic acid *(*142.7 µL, 2.496 mmol, 3 equiv) as an additive to give 3,5-dimethylbenzoic acid (24.6 mg, 0.164 mmol, 20%) and 5-methylisophthalic acid (70.7 mg, 0.392 mmol, 47%).

3,5-Dimethylbenzoic acid [7]:

^{1}H NMR (400 MHz, $CDCl_3$) δ 7.74 (s, 2 H), 7.24 (s, 1H).

^{13}C NMR (100 MHz, $CDCl_3$) δ 172.5, 138.3, 135.6, 129.3, 128.0, 21.3.

HRMS for $C_9H_9O_2$ [M–H]$^-$ found 149.0609; calcd. 149.0608.

5-Methylisophthalic acid [9]:

^{1}H NMR (400 MHz, DMSO–d_6) δ 13.18 (s, 2H), 8.28 (s, 1H), 7.98 (s, 2H), 2.43 (s, 3H).

^{13}C NMR (100 MHz, DMSO–d_6) δ 166.7, 138.8, 133.9, 131.2, 127.3, 20.6.

HRMS for $C_9H_9O_4$ [M+H]$^+$ found 181.0496; calcd. 181.0495.

5 Homocoupling reactions

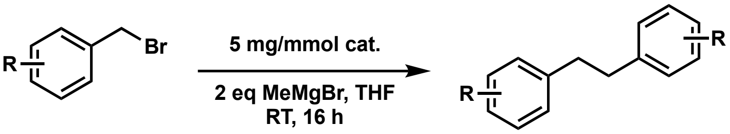

A solution of MeMgBr (3 M in Et_2O, 876 µL, 1.75 mmol, 2.0 equiv) was added dropwise into a solution of benzyl bromide (150 mg, 0.877 mmol, 1.0 equiv) and TAL–2–900 (4.4 mg) in THF (5 mL) at 0 °C, and the reaction was left to stir at RT. After 16 h, it was quenched with 1 M HCl, extracted with DCM and evaporated under reduced pressure to give the product as a colorless solid (76.3 mg, 0.419 mmol, 95%).

1,2-Diphenylethane [10]:

^{1}H NMR (400 MHz, $CDCl_3$) δ 7.34–7.30 (m, 4H), 7.25–7.21 (m, 6H), 2.96 (s, 4H).

^{13}C NMR (100 MHz, $CDCl_3$) δ 141.9, 128.6, 128.5, 126.0, 38.1.

A solution of MeMgBr (3 M in Et_2O, 600 µL, 1.20 mmol, 2.0 equiv) was added dropwise into a solution of 4-bromobenzyl bromide (150 mg, 0.600 mmol, 1.0 equiv) and TAL–2–900 (3.0 mg) in THF (5 mL) at 0 °C, and the mixture was left to stir at RT. After 16 h, it was quenched with 1 M HCl, extracted with DCM and evaporated under reduced pressure to give the product as a colorless solid (92.1 mg, 0.271 mmol, 90%).

1,2-Bis(4-bromophenyl)ethane [10]:

^{1}H NMR (400 MHz, $CDCl_3$) δ 7.38 (d, 4 H, J = 8.3), 7.00 (d, 4H, J = 8.3), 2.85 (s, 4H).

^{13}C NMR (100 MHz, $CDCl_3$) δ 140.2, 131.6, 130.4, 120.0, 37.2.

A solution of MeMgBr (3 M in Et_2O, 337 µL, 1.01 mmol, 2.0 equiv) was added dropwise into a solution of 4-iodobenzyl bromide (150 mg, 0.505 mmol, 1.0 equiv) and TAL–2–900 (2.5 mg) in THF (5 mL) at 0 °C, and the mixture was left to stir at RT. After 16 h, it was quenched with 1 M HCl, extracted with DCM and evaporated under reduced pressure to give the product as a colorless solid (101.3 mg, 0.233 mmol, 92%).

1,2-Bis(4-iodophenyl)ethane:

^{1}H NMR (400 MHz, $CDCl_3$) δ 7.59 (d, 4H, J = 8.3), 6.88 (d, 4H, J = 8.3), 2.83 (s, 4H).

^{13}C NMR (100 MHz, $CDCl_3$) δ 140.8, 137.4, 130.6, 91.2, 37.1.

HRMS for $C_{14}H_{13}I_2$ $[M+H]^+$ found 434.9058; calcd. 434.9107.

A solution of MeMgBr (3 M in Et_2O, 540 µL, 1.62 mmol, 2.0 equiv) was added dropwise into a solution of 4-iodobenzyl bromide (150 mg, 0.811 mmol, 1.0 equiv) and TAL–2–900 (4.1 mg) in THF (5 mL) at 0 ºC, and the mixture was left to stir at RT. After 16 h, it was quenched with 1 M HCl, extracted with DCM and evaporated under reduced pressure to give the product as a colorless solid (79.1 mg, 0.376 mmol, 93%).

1,2-Di-p-tolylethane [10]:

^{1}H NMR (400 MHz, $CDCl_3$) δ 7.17 (s, 8H), 2.95 (s, 4H), 2.41 (s, 6H).

^{13}C NMR (100 MHz, $CDCl_3$) δ 139.0, 135.4, 129.1, 128.4, 27.8, 21.1.

A solution of MeMgBr (3 M in Et_2O, 529 µL, 1.59 mmol, 2.0 equiv) was added dropwise into a solution of 2-fluorobenzyl bromide (150 mg, 0.794 mmol, 1.0 equiv) and TAL-2-900 (4.0 mg) in THF (5 mL) at 0 ºC, and the mixture was left to stir at RT. After 16 h, it was quenched with 1 M HCl, extracted with DCM and evaporated under reduced pressure to give the product as a colorless solid (65.2 mg, 0.299 mmol, 75%).

1,2-Bis(2-fluorophenyl)ethane:

^{1}H NMR (400 MHz, $CDCl_3$) δ 7.21–7.11 (m, 4H), 7.05–6.99 (m, 4H), 2.95 (s, 4H).

^{13}C NMR (100 MHz, $CDCl_3$) δ 161.3 (d, J_{CF} = 243), 130.9 (d, J_{CF} = 5), 128.4 (d, J_{CF} = 15), 127.9 (d, J_{CF} = 8), 124.0 (d, J_{CF} = 3), 115.3 (d, J_{CF} = 22), 29.9.

^{19}F NMR (376 MHz, $CDCl_3$) δ -119.0 – -119.1 (m).

A solution of MeMgBr (3 M in Et_2O, 326 µL, 0.977 mmol, 2.0 equiv) was added dropwise into a solution of 2-fluorobenzyl bromide (150 mg, 0.489 mmol, 1.0 equiv) and TAL–2–900 (2.4 mg) in THF (5 mL) at 0 ºC, and the mixture was left to stir at RT. After 16 h, it was quenched with 1 M HCl, extracted with DCM and evaporated under reduced pressure to give the product as a colorless solid (101.2 mg, 0.223 mmol, 91%).

1,2-Bis(3,5-bis(trifluoromethyl)phenyl)ethane:

^{1}H NMR (400 MHz, $CDCl_3$) δ 7.76 (s, 2H), 7.58 (s, 4H), 3.11 (s, 4H).

^{13}C NMR (100 MHz, $CDCl_3$) δ 142.7, 132.1 (q, J_{CF} = 33), 128.8 (d, J_{CF} = 2), 123.4 (q, J_{CF} = 271, CF_3), 120.8 (p, J_{CF} = 4), 37.1.

^{19}F NMR (376 MHz, $CDCl_3$) δ –63.0.

A solution of MeMgBr (3 M in Et_2O, 383 µL, 1.15 mmol, 2.0 equiv) was added dropwise into a solution of 2-fluorobenzyl bromide (150 mg, 0.575 mmol, 1.0 equiv) and TAL–2–900 (2.9 mg) in

THF (5 mL) at 0 ºC, and the mixture was left to stir at RT. After 16 h, it was quenched with 1 M HCl, extracted with DCM, evaporated under reduced pressure to give the product as a colorless solid (100.7 mg, 0.278 mmol, 97%).

1,2-Bis(perfluorophenyl)ethane [10]:

^{1}H NMR (400 MHz, $CDCl_3$) δ 3.02 (s, 4H).

^{13}C NMR (100 MHz, $CDCl_3$) δ 146.6–146.4 (m), 141.6–141.4 (m), 136.5–136.2 (m), 113.1–112.7 (m), 22.0.

^{19}F NMR (376 MHz, $CDCl_3$) δ –144.3 to –144.4 (m), –155.9 (t, J = 20.6), –162.0 to –162.2 (m).

6 Electrochemical measurements

The electrochemical activity of TAL–2 derived catalyst materials was assessed using Autolab electrochemical workstation equipped with rotating disk electrode (RDE). A three-neck electrochemical glass cell was used in all RDE experiments. Glassy carbon (GC) electrode with diameter of 5 mm mounted into a Teflon holder served as working electrode. GC rod and reversible hydrogen electrode (RHE) were counter and reference electrodes, respectively.

Catalyst powder was ultrasonically dispersed in 0.05 wt% Nafion solution in 2-propanol and deposited onto the GC surface to yield a catalyst loading of 0.50 mg cm^{-2}. For comparison, commercial Pt/C (E-TEK, loading 0.10 mg cm^{-2}) was used as a reference for the ORR and HER, while RuO_2 was used as a reference for the OER (Alfa Aesar, loading 0.12 mg cm^{-2}). For experiments in alkaline and acid media 0.1 M KOH and 0.5 M H_2SO_4 electrolyte solutions were used, respectively.

ORR. First, cyclic voltammetry (CV) experiments were performed to obtain stable catalyst surface. Catalysts were cycled for at least 5 times in argon-saturated electrolyte solution between –0.1 and 1.1 V *vs.* RHE at 50 mV s^{-1}. (Pt/C benchmark was cycled between 0.1 and 1.4 V vs RHE and CO-stripping voltammetry was performed in order to obtain clean Pt surface). Then a background CV was recorded at 10 mV s^{-1}.

ORR experiments were performed in O_2-saturated electrolyte and RDE polarization curves were recorded at a scan rate of 10 mV s^{-1} at different electrode rotation speeds (360, 610, 960, 1600, 1900, 3100 rpm). The background current was then subtracted from the RDE data in order to eliminate capacitive current contribution.

The data obtained from RDE polarization curves was analyzed by the Koutecky–Levich (K–L) equation (1) [11]:

$$\frac{1}{j} = \frac{1}{j_{\mathrm{k}}} + \frac{1}{j_{\mathrm{d}}} = -\frac{1}{nFkC_{O_2}^{b}} - \frac{1}{0.62nFD_{O_2}^{2/3}\nu^{-1/6}C_{O_2}^{b}\omega^{1/2}} \qquad (1)$$

where j, j_{k} and j_{d} – are measured, kinetic and diffusion-limited current densities, respectively, n is the amount of electrons transferred per oxygen molecule, k is the electrochemical rate constant for

O_2 reduction (cm s^{-1}), *F* is the Faraday constant (96,485 C mol^{-1}), ω is the electrode rotation rate (rad s^{-1}), C_{O2}^b is the concentration of oxygen in the bulk (1.2×10^{-6} mol cm^{-3}) [12], D_{O2} is the diffusion coefficient of O_2 (1.9×10^{-5} cm^2 s^{-1}) [13] and v is the kinematic viscosity of the solution (0.01 cm^2 s^{-1}) [13].

RRDE analysis was performed to determine the ORR pathway. The hydrogen peroxide yield and electron transfer number (n) was calculated based on the following equations (2) and (3):

$$\%[\mathrm{HOO^-}] = \frac{\frac{2I_\mathrm{r}}{N}}{I_\mathrm{d} + \frac{I_\mathrm{r}}{N}} \times 100\% \tag{2}$$

$$n = \frac{4I_\mathrm{d}}{I_\mathrm{d} + \frac{I_\mathrm{r}}{N}} \tag{3}$$

where I_d is the disk current, I_r is the ring current and *N* is collection efficiency of the gold ring electrode (N = 0.22).

To explore the ORR stability of TAL-2-derived catalyst materials, the electrode potential was cycled 5000 times between 0.6 and 1.0 V vs. RHE in O_2-saturated electrolyte at 100 mV s^{-1} (rotated at 1600 rpm) and RDE curves before and after stability test were compared.

OER. To obtain OER data LSV curves were recorded at 1600 rpm in 0.1 M KOH electrolyte using a scan rate of 10 mV s^{-1} in potential window of 1–1.8 V vs. RHE. Before measurement electrode was cycled 40 times at the scan rate of 200 mV/s to activate the material. Catalyst durability was evaluated by recording the chronoamperometry (i–t) curve at the potential of 1.6 V at 1600 rpm. Electrochemical impedance spectroscopy was performed in order to obtain iR-compensated potentials.

HER. HER measurements were performed in argon-saturated 1 M KOH solution. HER was measured also in 0.5 M H_2SO_4 solution. Before measurement electrodes were cycled 5 times at scan rate of 50 mV s^{-1} and stable LSV was recorded at 10 mV s^{-1} within the potential range of –0.8 to 1 V vs RHE.

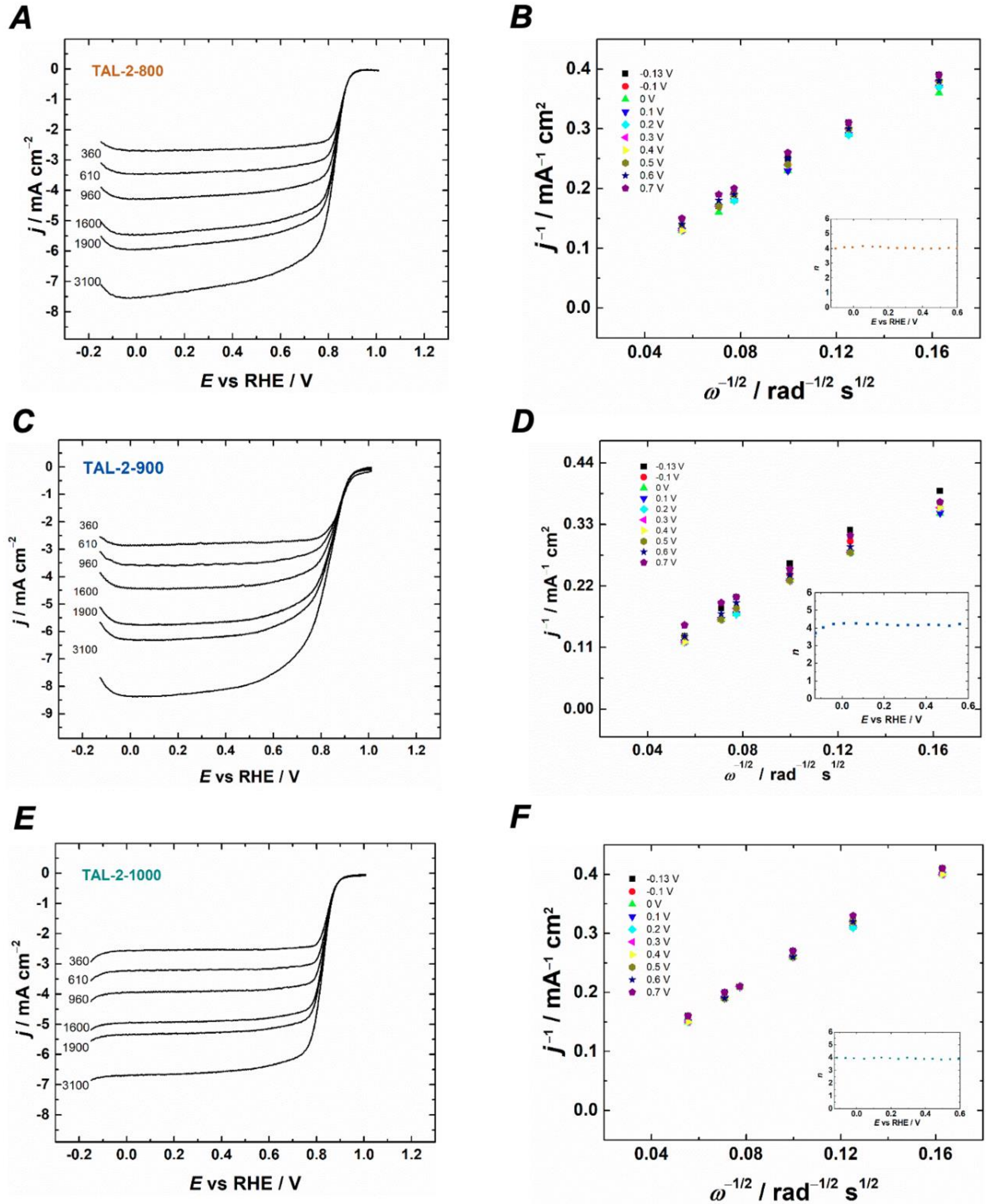

Figure S4. RDE polarization data on oxygen reduction recorded at various rotation rates on (A) TAL–2–800, (C) TAL–2–900 and (E) TAL-2-1000 modified GC electrode; ν = 10 mV s $^{-1}$. Koutecky−Levich plots for O_2 reduction on (B) TAL–2–800, (D) TAL–2–900 and (F) TAL–2–1000 modified GC electrode. Insets: potential dependence of the number of electrons transferred per O_2 molecule.

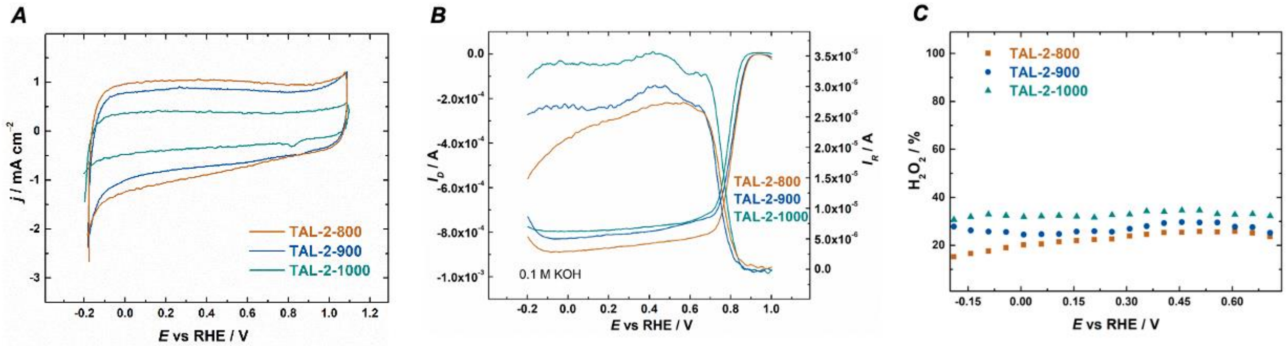

Figure S5. Electrochemical characterization of TAL–2 derived materials in 0.1 M KOH. (A) Cyclic voltammograms of electrocatalyst-modified GC electrodes (under argon); ν = 50 mV s^{-1}. (B) RRDE polarization curves. (C) H_2O_2 production percentages.

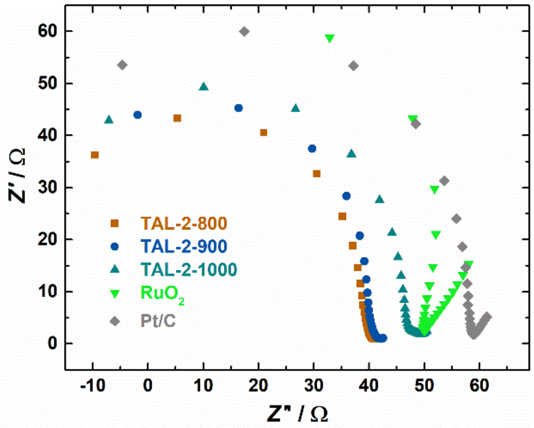

Figure S6. The Nyquist plots.

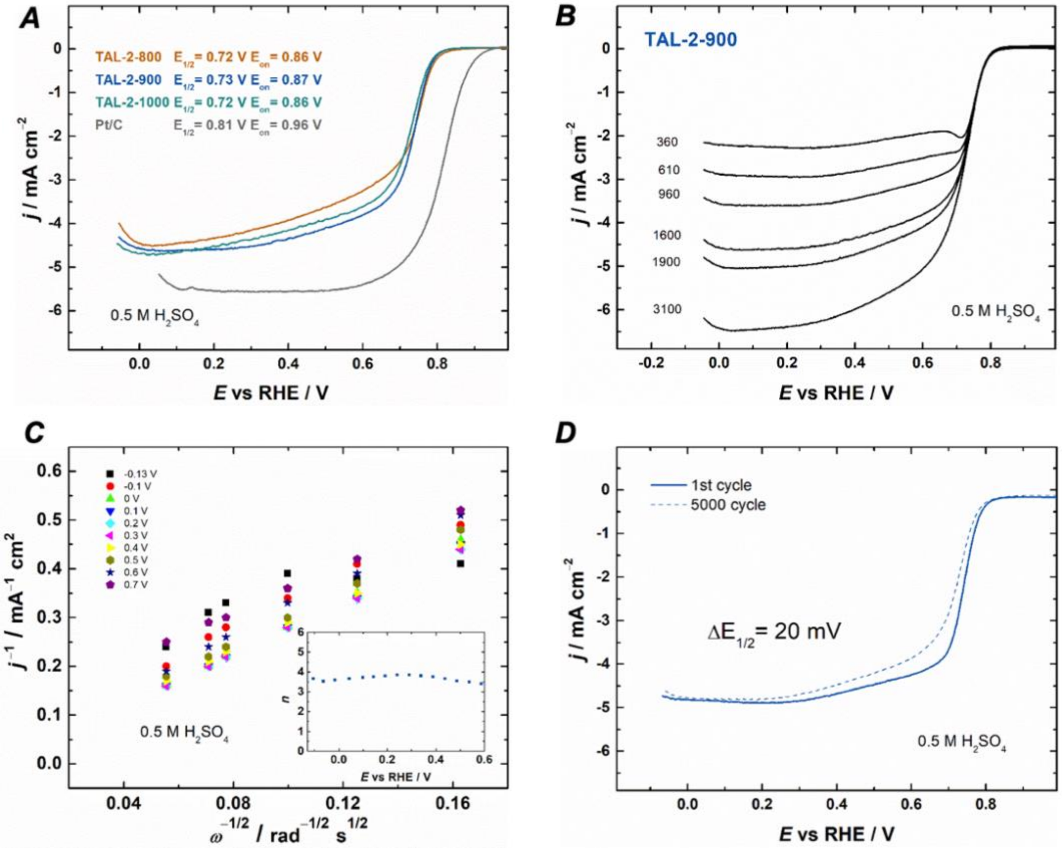

Figure S7. Electrochemical oxygen reduction on TAL materials in 0.5 M H_2SO_4. (A) RDE polarization curves for TAL–2 derived and Pt/C-modified GC electrodes at 1600 rpm; ν = 10 mV s $^{-1}$. (B) RDE polarization data on oxygen reduction recorded at various rotation rates on TAL–2–900 modified GC electrode; ν = 10 mV s $^{-1}$. (C) Koutecky−Levich plots for O_2 reduction on TAL–2–900 modified GC electrode. Inset: number of electrons transferred per O_2 molecule. (D) Electrochemical stability test for TAL–2–900 (mid-range: 0.6−1.0 V).

Table S9. Comparison of various parameters for trifunctional ORR/OER/HER catalysts.

entry	*catalyst*	*precursors*	*catalyst loading* mg cm $^{-2}$	*ORR* $E_{1/2}$ @−3 mA cm^{-2} @1600 rpm	*OER* E_{10} @10mA cm^{-2} @1600 rpm	*ΔE*	*HER* $-E_{-10}$ @10 mA cm^{-2} @1600 rpm	*reference*
cobalt-based materials								
1	**Co/MMCs**	PPy + carbon fibers + CoCl$_2$	0.22	0.84 (1 M KOH)	1.41 (1 M KOH)	0.57	0.086 (1 M KOH)	[14]
2	**Co/CNFs (1000)**	Co foil + melamine	0.3	0.896 (0.1 M KOH)	1.55 (1 M KOH)	0.65	0.19 (1 M KOH)	[15]
3	**Co$_2$B/Co/N-B-C/B$_4$C**	B$_4$C + Co(OAc)$_2$ + melamine	0.127	0.83 (0.1 M KOH)	1.53 (0.1 M KOH)	0.70	0.22 (0.1 M KOH)	[16]
4	**CoT@NC**	NH$_4$@Zn$_3$OH(PzC)$_3$	0.2	0.86 (0.1 M KOH)	1.58 (1 M KOH)	0.72	0.209 (1 M KOH)	[17]
5	**Co$_4$N@NC-2**	ZIF-67	0.3	0.84 (0.1 M KOH)	1.52 (0.1 M KOH)	0.68	0.283 (1 M KOH)	[18]
6	**Co@N-C-800**	THB + Co(OAc)$_2$	0.36	0.85 (0.1 M KOH)	1.58 (1 M KOH)	0.73	0.292 (0.5 M H$_2$SO$_4$)	[19]
7	***TAL-2-900***	***CoCl$_2$ + L1***	***0.50***	***0.85 (0.1 M KOH)***	***1.60 (0.1 M KOH)***	***0.75***	***0.264 (1 M KOH)*** ***0.289 (0.5 M H$_2$SO$_4$)***	***This work***
8	**Co@N-CNTF**	Co(OAc)$_2$ + adenine	0.28	0.81 (0.1 M KOH)	1.58 (1 M KOH)	0.77	0.26 (1 M KOH)	[20]
9	**Co/NGC-3**	g-C$_3$N$_4$ + glucose + ZIF-67	0.20	0.85 (0.1 M KOH)	1.636 (0.1 M KOH)	0.786	0.293 (0.1 M KOH)	[21]
10	**D–Co@CNG**	GO + Co(NO$_3$)$_2$ + Zn(NO$_3$)$_2$ + 2-MIM	0.20	0.81 (0.1 M KOH)	1.60 (1 M KOH)	0.79	0.205 (1 M KOH)	[22]
11	**Co/CoO@Co–N-C-800**	shrimp-shell + Co(NO$_3$)$_2$ + pyrrole	0.305	0.854 (0.1 M KOH)	1.664 (0.1 M KOH)	0.81	0.376 (0.1 M KOH) (@20 mA cm^{-2})	[23]
12	**Co$_2$P**	Co(acac)$_2$ + TOP	0.2	0.839 (0.1 M KOH)	1.51 (1 M KOH)	0.671	0.075 (1 M KOH)	[24]
13	**CoP NPs/CNSs**	Co(OAc)$_2$ + melamine + phytic acid	0.25	0.88 (0.1 M KOH)	1.58 (1 M KOH)	0.7	0.115 (1 M KOH)	[25]
14	**Co$_2$P/CoNPC**	ZIF-67 + red phosphorus	0.39	0.843 (0.1 M KOH)	1.556 (1 M KOH)	0.713	0.28 (1 M KOH)	[26]
15	**Co$_2$P/NPG–900**	CoPc(NH$_2$)$_4$ + GO + Cl$_6$N$_3$P$_3$	0.254	0.81 (0.1 M KOH)	1.55 (1 M KOH)	0.74	0.245 (1 M KOH)	[27]
16	**CoP@SNC**	Co(Ac)$_2$·+ HEDP	0.6	0.79 (0.1 M KOH)	1.58 (1 M KOH)	0.79	0.174 (1 M KOH)	[28]
17	**Co$_2$P/CoN in NCNTs**	melamine + P123 + TPP + Co(NO$_3$)$_2$	0.1	0.85 (0.1 M KOH)	1.65 (0.1 M KOH)	0.80	0.098 (0.5 M H$_2$SO$_4$)	[29]
18	**CoP-PBSCF**	NaH$_2$PO$_2$·H$_2$O + H-PBSCF	0.255	0.752 (0.1 M KOH)	1.57 (0.1 M KOH)	0.81	0.24 (0.1 M KOH)	[30]
19	**Co-B-O/NPC–50%**	Co(Ac)$_2$+ NaBH$_4$ + lecithin + g-C$_3$N$_4$	0.42	0.83 (0.1 M KOH)	1.58 (1 M KOH)	0.753	0.316 (1 M KOH)	[31]

20	**CoSA+Co_9S_8/HCNT**	ZnS + ZIF-67 + polydopamine	NA	0.855 (0.1 M KOH)	1.56 (0.1 M KOH)	0.705	0.25 (1 M KOH)	[32]
21	**NS/rGO-Co_4**	Co(NO_3)2 + thiourea + GO + sodium dodecyl benzene sulfonate (SDBS)	0.404	0.79 (0.1 M KOH)	1.495 (0.1 M KOH)	0.705	0.15 (0.5 M H_2SO_4)	[33]
22	**$Co_{0.85}$Se@NC**	ZIF-67 + Se	0.20	0.817 (0.1 M KOH)	1.55 (1 M KOH)	0.733	0.230 (1 M KOH)	[34]
23	**DAP–DAB–Co(OAc)$_2$·4H_2O**	DAP +DAB + Co(OAc)$_2$	0.30	0.90 (0.1 M KOH)	1.62 (0.1 M KOH)	0.72	0.20 (1 M KOH)	[35]
24	**CF–NG–Co**	Co(Ac)$_2$ + GO + melamine	0.28	0.88 (0.1 M KOH)	1.63 (1 M KOH)	0.75	0.212 (1 M KOH)	[36]
iron-based materials								
25	**BA-TAP-Fe-800**	2,4,6-triaminopyrimidine + barbituric acid + $FeCl_3$	0.283	0.85 (0.1 M KOH)	1.55 (0.1 M KOH)	0.7	0.33 (0.1 M KOH)	[37]
26	**FeP_x/Fe-N-C/NPC**	tannic acid + $FeCl_2$·4H_2O + Na_2HPO_4	0.21/0.42 (HER)	0.86 (0.1 M KOH)	1.565 (1 M KOH)	0.705	0.075 (0.5 M H_2SO_4)	[38]
27	**PPy/FeTCPP/Co**	pyrrole + FeTCPP + Co(NO_3)$_2$	0.3	0.86 (0.1 M KOH)	1.61 (0.1 M KOH)	0.75	0.24 (0.1 M KOH)	[39]
28	**FeS/Fe_3C@N-S-C-800**	benzenetricarboxylic acid + Pd(PPh_3)$_4$ + 3,8-DBPT-dibromophenanthroline + Fe(OAc)$_2$ + DMSO	0.3/0.6	0.87 (0.1 M KOH)	1.80 (1 M KOH)	0.93	0.174 (0.5 M H_2SO_4)	[40]
other metal based materials [Ni, W, Ru, Mo]								
29	**Ni-NC700**	Ni(NO_3)$_2$+ 2,6-pyridine dicarboxylic acid + 4,4′-bipy	0.31	0.75 (0.1 M KOH)	1.66 (0.1 M KOH)	0.91	0.301 (0.1 M KOH)	[41]
30	**W_2N/WC**	WO_3 powder + dicyanodiamide	0.20	0.83 (0.1 M KOH)	1.56 (1 M KOH)	0.73	0.148 (1 M KOH)	[42]
31	**Ru-SA/$Ti_3C_2T_x$**	Ti_3AlC_2 + $RuCl_3$	0.61	0.80 (0.1 M $HClO_4$)	1.53 (0.1 M $HClO_4$)	0.73	0.07 (0.5 M H_2SO_4)	[43]
32	**G@N-MoS_2**	sulfur + $MoCl_5$ + MgO + NH_3	0.25	0.716 (0.1 M KOH)	1.63 (0.1 M KOH)	0.914	0.243 (0.5 M H_2SO_4)	[44]
multi-transition-metals based materials								
33	**CoO_x-NeC/TiO_2C (22.7%)**	$Ti_3C_2T_x$ + Co(NO_3)$_2$ + Zn(NO_3)$_2$ + 2-MIM	0.141	0.85 (0.1 M KOH)	1.58 (1 M KOH)	0.72	0.367 (1 M KOH)	[45]
34	**N/CF-EC-900**	Co(NO_3)$_2$ + Fe(NO_3)$_3$ + albumin	0.17	0.849 (0.1 M KOH)	1.61 (0.1 M KOH)	0.761	0.164 (0.1 M KOH)	[46]
35	**IrO_2-ZnO**	$ZnCl_2$ + $IrCl_3$ + NH_3	0.2547	0.81 (1 M KOH)	1.59 (1 M KOH)	0.78	0.25 (1 M KOH)	[47]
36	**ZnCo−PVP-900**	Zn(NO_3)$_2$ + K_3Co(CN)$_6$ + PVP	0.28	0.83 (0.1 M KOH)	1.63 (1 M KOH)	0.80	0.25 (1 M KOH)	[48]
37	**Co_2Mn_1 DH**	Mn(NO_3)$_2$ + Co(NO_3)$_2$	0.25	0.78 (0.1 M KOH)	1.58 0.1 M KOH	0.80	0.187 (1 M KOH)	[49]
38	**Ni_2P/CoN-PCP**	$NiCl_2$ + CoN–PCP support + NaH_2PO_2 +	0.26	0.871 (0.1 M KOH)	1.50 (1 M KOH)	0.629	0.094 (1 M KOH)	[50]
39	**NiCoP/CNF-900**	polyacrylonitrile + Ni(NO_3)$_2$ + Co(NO_3)$_2$ + red P	NA	0.82 (0.1 M KOH)	1.508 (1 M KOH)	0.688	0.130 (1 M KOH)	[51]
40	**FeNi@N-CNT/NCSs**	g-C_3N_4 + aniline + Fe(NO_3)$_3$ + Ni(NO_3)$_2$	0.255	0.84 (0.1 M KOH)	1.59 (0.1 M KOH)	0.75	0.203 (1 M KOH)	[52]
41	**Pt/NiO/Ni/CNT-3**	CNTs + Zn plate + $NiCl_2$ + K_2PtCl_6	0.255	0.94 (0.1 M KOH)	1.7 (0.1 M KOH)	0.76	0.117 (0.1 M KOH)	[53]

42	**$CoP/Ni_2P@NC$**	$CoCl_2·6H_2O$ + $NiCl_2·6H_2O$ + EDTMPS	NA	0.79 (0.1 M KOH)	1.57 (1 M KOH)	0.78	0.330 (1 M KOH)	[54]
43	**NiCoOS**	ZIF-67 + $Ni(NO_3)_2·6H_2O$ + thioacetamide	0.318	0.79 (0.1 M KOH)	1.7 (0.1 M KOH)	0.91	0.3 (0.1 M KOH)	[55]
44	**$FeCo/Co_2P@NPCF$**	bacterial cellulose + $K_3[Fe(CN)_6]$ + $CoCl_2$ + melamine + phytic acid	0.28	0.79 (0.1 M KOH)	1.56 (0.1 M KOH)	0.77	0.26 (1 M KOH)	[56]
45	**Rh_6Cu_1/C**	$RhCl_3$ + $CuCl_2$+ PVP + ascorbic acid	0.282	0.85 (0.1 M KOH)	1.54 (1 M KOH)	0.69	0.017 (0.5 M H_2SO_4)	[57]
46	**$Co_9S_8@MoS_2$**	$Co(OAc)_2$ + Na_2MoO_4 + PVP	0.407	0.88 (0.1 M KOH)	1.57 (1 M KOH)	0.69	0.143 (1 M KOH)	[58]
47	**$O\text{-}Co_{0.5}Mo_{0.5}Se_2$**	nickel foam + $Co(NO_3)_2$ + Na_2MoO_4 + hexamethylenetetramine + Se	NA	0.83 (0.1 M KOH)	1.406 (1 M KOH)	0.576	0.102 (1 M KOH)	[59]
48	**$Co_9S_8\text{-}MoS_2/N\text{-}CNAs@CNFs$**	$Zn(NO_3)_2$ + $Co(NO_3)_2$ + 2-MIM + Na_2MoO_4	0.17	0.82 (0.1 M KOH)	1.57 (1 M KOH)	0.75	0.163 (1 M KOH)	[60]
49	**$Co_{5.47}N@Co_3Fe_7/N\text{-}C$**	Urea + GO + oxidized CNTs + $FeCl_3$ + $CoCl_2$	0.60	0.94 (0.1 M KOH)	1.72 (0.1 M KOH)	0.78	0.181, (1 M KOH) 0.115, (0.5 M H_2SO_4)	[61]
50	**Cu-foam@CuCoNC–500**	$Cu(OH)_2$ + Cu foam + $Co(NO_3)$ + dimethylimidazole	NA	0.84 (0.1 M KOH)	1.485 (1 M KOH)	0.645	0.059 (1 M KOH)	[62]
51	**$Fe_3C\text{-}Co/NC$**	P123 + $Co(NO_3)_2$ + $Fe(NO_3)_3$ + melamine	0.2 ORR 0.4 OER 0.3 HER	0.885 (0.1 M KOH)	1.58 (1 M KOH)	0.695	0.238 (1 M KOH)	[63]
non-metal based materials								
52	**SHG**	melamine + $NiSO_4$ + KCl	0.71	0.87 (0.1 M KOH)	1.60 (0.1 M KOH)	0.73	0.31 (0.1 M KOH)	[64]
53	**NOGB-800**	sodium citrate + $Co(NO_3)_2$ + $K_3[Fe(CN)_6]$ + dopamine	0.4	0.84 (0.1 M KOH)	1.65 (1 M KOH)	0.81	0.22 (1 M KOH)	[65]
54	**N-doped graphene**	graphene + melamine	0.283	0.76 (0.1 M KOH)	1.57 (1 M KOH)	0.81	0.15 (0.5 M H_2SO_4)	[66]
55	**NCN-1000-5**	citric acid + NH_4Cl	0.2	0.82 (0.1 M KOH)	1.64 (0.1 M KOH)	0.82	0.09 (0.5 M H_2SO_4)	[67]

PPy = polypyrrole nanowires , THB = 1, 3, 5-tris (4′-hydroxy-5′-formylphenyl) benzene, TOP = trioctylphosphine, HEDP = 1-hydroxyethylidene-1,1-diphosphonic acid, CoP-PBSCF = The CoP-$PrBa_{0.5}Sr_{0.5}Co_{1.5}Fe_{0.5}O_{5+\delta}$, EDTMPS = sodium salt of ethylenediamine tetra(methylenephosphonicacid), DAP = 2,6-diacetylpyridine, DAB = 3,3′-diaminobenzidine, TCPP = tetra(4-carboxyphenyl)porphyrin, PVP = polyvinylpyrrolidone

Table S10. Comparison of the main ORR/OER/HER kinetic parameters obtained for TAL-2 derived catalyst materials.

catalyst	ORR		OER			HER	
	E_{onset} @1600 rpm V vs. RHE	$E_{1/2}$ @–3mA cm^{-2} 1600 rpm V vs. RHE	E_{10} @10mA cm^{-2}@1600rpm V	η mV	ΔE V	η mV	ECSA
TAL-2-800	0.96	0.83	1.69	460	0.86	417	440
TAL-2-900	1.00	0.85	1.60	370	0.75	264	366
TAL-2-1000	0.97	0.83	1.65	420	0.82	411	178
Pt/C	1.01	0.86	n.a.	n.a.	n.a.	57	n.a.
RuO_2	n.a.	n.a.	1.69	n.a.	n.a.	n.a.	n.a.

Table S11. Specific surface area and porosity related parameters derived from N_2 physisorption analysis.

material	S_{BET} $m^2\ g^{-1}$	S_{DFT} $m^2\ g^{-1}$	V_{tot} $cm^3\ g^{-1}$	V_{μ} $cm^3\ g^{-1}$
TAL-2	59	41	0.09	0.01
TAL-2-800	589	655	0.55	0.2
TAL-2-900	421	441	0.39	0.14
TAL-2-1000	394	372	0.44	0.11

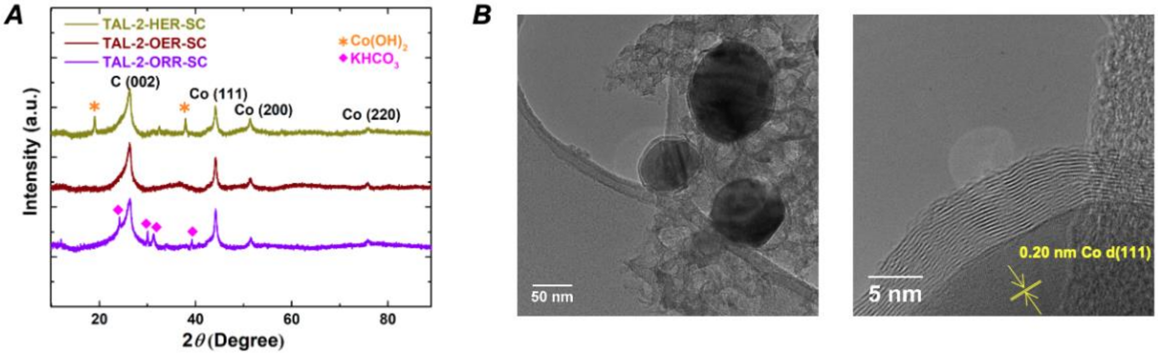

Figure S8. (A) PXRD patterns of spent TAL–2–900 catalysts (SC) after ORR, OER and HER stability tests. (B) HRTEM micrograph of spent catalyst after ORR.

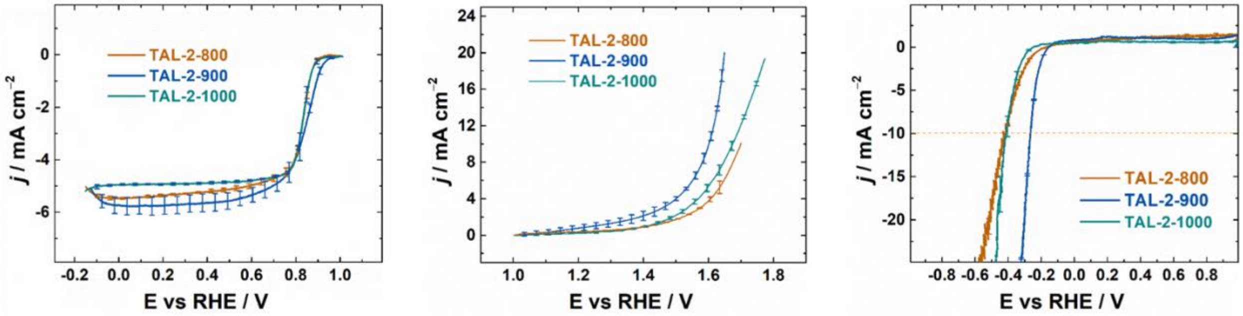

Figure S9. Reproducibility of TAL-2 derived materials in ORR, OER and HER. All experiments were conducted six times individually using different batches of the catalyst materials.

7 AEMFC and ZAB Applications

Alkaline anion exchange membrane fuel cell (AEMFC). For the preparation of membrane electrode assembly (MEA) TAL–2–900 (2 mg cm^{-2}) was applied on the cathode and Pt-Ru/C (loading 0.6 mg cm^{-2}) was used as anode catalyst. Poly[2,2′-(2,2″,4,4″,6,6″-hexamethyl-p-terphenyl-3,3″-diyl)-5,5′-bibenzimidazole] (HMT–PMBI) placed between two gas diffusion layers (GDL) modified with catalyst material. HMT–PMBI was also used as ionomer in the catalyst ink to enhance ink stability of gas diffusion layers. The ink suspension was prepared using 1% solid catalyst (catalyst/HMT–PMBI 85:15) disseminated in 99% of mixture of methanol/water (CH_3OH/H_2O 3:1) for both cathode and anode. The ink was sonicated for an hour before modifying the GDLs. A cut piece (square shape; 4 cm^2) of HMT–PMBI membrane was soaked in 1 M KOH along with modified GDLs for 24 h. The AEMFC hardware was assembled placing HMT–PMBI between catalyst modified GDLs with PTFE gasket using torque of 5 Nm. The area of the fuel cell electrode was 5 cm^2. The single cell fuel cell test was performed with Greenlight Fuel Cell Test Station (G50 Fuel cell system, Hydrogenics, Vancouver, Canada) using humidified H_2 and O_2 gases at 60 ^{o}C with back pressure of 190–200 kPa for cathode and anode. The flow rates of H_2 and O_2 were 0.30 and 0.35 L min^{-1}, respectively.

Zinc–air battery (ZAB). *Preparation of PVA gel electrolyte:* Polymer electrolyte was prepared according to the previously reported procedure [68]. Under optimized conditions, poly(vinyl) alcohol (5 g, M_w ~ 145k, Mowiol® 28–99) was added into a solution of $Zn(OAc)_2$ in 0.1 M KOH (100 mL) and the mixture was left to stir at 90 ^{o}C. After 90 min, 24 mL of the mixture was poured into a Petri dish (⌀10 cm) and left to gelate by storing at –20 ^{o}C for 3 h to give the desired gel electrolyte.

ZAB preparation and testing: Zinc foil (0.03 mm thickness) and carbon cloth (carbon loading of 30 g/m^2) were used without additional treatment. A suspension of TAL–2–900 (10 mg) and Nafion (10 µL of a 0.5% stock solution) in 2-propanol (1 mL) was sonicated for 1 h. It was then pipetted onto the carbon cloth (square; 2 cm × 2 cm). A sandwich-like ZAB (final catalyst loading: 2.5 mg/cm^2) was tested under indicated potential until the loss of activity.

References

[1] Gottlieb, H. E.; Kotlyar, V.; Nudelman, A. NMR chemical shifts of common laboratory solvents as trace impurities. *J. Org. Chem*. **1997**, *62*, 7512–7515. DOI:10.1021/jo971176v

[2] Jiang, H.; Ruokolainen, J.; Young, N.; Oikawa, T.; Nasibulin, A. G.; Kirkland, A.; Kauppinen, E. I. Performance and early applications of a versatile double aberration-corrected JEOL-2200FS FEG TEM/STEM at Aalto University. *Micron* **2012**, *43*, 545–550. DOI:10.1016/j.micron.2011.10.004

[3] Brunauer, S.; Emmett, P. H.; Teller, E. Adsorption of gases in multimolecular layers. *J. Am. Chem. Soc*. **1938**, *60*, 309–319. DOI:10.1021/ja01269a023

[4] Young, J. A. Benzoic acid. *J. Chem. Educ.* **2006**, *83*, 697. DOI:10.1021/ed083p697

[5] Yuan, Y.; Shi, X.; Liu, W. Transition-metal-free, chemoselective aerobic oxidations of sulfides and alcohols with potassium nitrate and pyridinium tribromide or bromine. *Synlett* **2011**, *4*, 559–564. DOI:10.1055/s-0030-1259516

[6] Schmidt, A. K.; Stark. C. B. W. TPAP-catalyzed direct oxidation of primary alcohols to carboxylic acids through stabilized aldehyde hydrates. *Org. Lett*. **2011**, *13*, 4164–4167. DOI:10.1021/ol2014335

[7] Yang, D.; Yang, H.; Fu, H. Copper-catalyzed aerobic oxidative synthesis of aromatic carboxylic acids. Chem. Commun. **2011**, *47*, 2348-2350. DOI:10.1039/C0CC04319B

[8] Crisostomo, C.; Crestani, M. G.; Garcia, J. J. The catalytic hydration of 1,2-, 1,3- and 1,4-dicyanobenzenes using nickel(0) catalysts. *J. Mol. Catal.* **2007**, *266*, 139–148. DOI:10.1016/j.molcata.2006.10.054

[9] Schorger, A. W. The action of aluminum chloride on cymene. *J. Am. Chem. Soc*. **1917**, *39*, 2671–2679. DOI:10.1021/ja02257a019

[10] Sato, K.; Inoue, Y.; Mori, T.; Sakaue, A.; Tarui, A.; Omote, M.; Kumadaki, I.; Ando, A. Csp^3–Csp^3 homocoupling reaction of benzyl halides catalyzed by rhodium. *Org. Lett.* **2014**, *16*, 3756–3759. DOI:10.1021/ol501619w

[11] Bard, A. J.; Faulkner, L. R. *Electrochemical Methods: Fundamental and Applications*, 2nd ed. Wiley, New York, **2001**.

[12] Davis, R. E.; Horvath, G. L.; Tobias, C. W. The solubility and diffusion coefficient of oxygen in potassium hydroxide solutions. *Electrochim. Acta* **1967,** *12*, 287–297. DOI:10.1016/0013-4686(67)80007-0

[13] Lide, D. R. *CRC Handbook of Chemistry and Physics*, CRC Press, Boca Raton, **2001**, pp. 1995–1996.

[14] Huang, N.; Yang, L.; Zhang, M.; Yan, S.; Ding, Y.; Sun, P.; Sun, X. Cobalt-embedded N-doped carbon arrays derived in situ as trifunctional catalyst toward hydrogen and oxygen evolution, and oxygen reduction. *ChemElectroChem* **2019**, *6*, 4522–4532. DOI:10.1002/celc.201901106

[15] Yang, Z.; Zhao, C.; Qu, Y.; Zhou, H.; Zhou, F.; Wang, J.; Wu, Y.; Li, Y. Trifunctional self-supporting cobalt-embedded carbon nanotube films for ORR, OER, and HER triggered by solid diffusion from bulk metal. *Adv. Mater*. **2019**, *31*, 1808043. DOI:10.1002/adma.201808043

[16] Liu, X.; Wang, Y.; Chen, L.; Chen, P. Jia, S.; Zhang, Y.; Zhou, S.; Zang, J. Co_2B and Co nanoparticles immobilized on the N–B-doped carbon derived from nano-B_4C for efficient catalysis of oxygen evolution, hydrogen evolution, and oxygen reduction reactions. *ACS Appl. Mater. Interfaces* **2018**, *10*, 37067–37078. DOI:10.1021/acsami.8b13359

[17] Shi, M.; Wang, J.-H.; Zhang, Y.; Zhang, X.-M. A rational design of efficient trifunctional electrocatalysts derived from tailored Co^{2+}-functionalized anionic metal–organic frameworks. *Dalt. Trans.* **2020**, *49*, 2280–2289. DOI:10.1039/C9DT04930D

[18] Ge, H.; Li, G.; Shen, J.; Ma, W.; Meng, X.; Xu, L. Co_4N nanoparticles encapsulated in N-doped carbon box as tri-functional catalyst for Zn–air battery and overall water splitting. *Appl. Catal. B Environ.* **2020**, *275*, 119104. DOI:10.1016/j.apcatb.2020.119104

[19] Kong, F.; Fan, X.; Zhang, X.; Wang, L.; Kong, A.; Shan, Y. Soft-confinement conversion of Co-salen-organic-frameworks to uniform cobalt nanoparticles embedded within porous carbons as robust trifunctional electrocatalysts. *Carbon* **2019**, *149*, 471–482. DOI:10.1016/j.carbon.2019.04.079

[20] Guo, H.; Feng, Q.; Zhu, J.; Xu, J.; Li, Q.; Liu, S.; Xu, K.; Zhang, C.; Liu, T. Cobalt nanoparticle-embedded nitrogen-doped carbon/carbon nanotube frameworks derived from a metal–organic framework for trifunctional ORR, OER and HER electrocatalysis. *J. Mater. Chem. A* **2019**, *7*, 3664–3672. DOI:10.1039/C8TA11400E

[21] Li, J.; Kang, Y.; Liu, D.; Lei, Z.; Liu, P. Nitrogen-doped graphitic carbon-supported ultrafine co nanoparticles as an efficient multifunctional electrocatalyst for HER and rechargeable Zn–air batteries. *ACS Appl. Mater. Interfaces* **2020**, *12*, 5717–5729. DOI:10.1021/acsami.9b18101

[22] Huang, Y.; Liu, Q.; Lv, J.; Babu, D. D. Wang, W.; Wu, M.; Yuan, D.; Wang, Y. Co-intercalation of multiple active units into graphene by pyrolysis of hydrogen-bonded precursors for zinc–air batteries and water splitting. *J. Mater. Chem. A* **2017**, *5*, 20882–20891. DOI:10.1039/C7TA06677E

[23] Zhang, X.; Liu, R.; Zang, Y.; Liu, G.; Wang, G.; Zhang, Y.; Zhang, H.; Zhao, H. Co/CoO nanoparticles immobilized on Co–N-doped carbon as trifunctional electrocatalysts for oxygen reduction, oxygen evolution and hydrogen evolution reactions. *Chem. Commun.* **2016**, *52*, 5946–5949. DOI:10.1039/C6CC02513G

[24] Li, H.; Li, Q.; Wen, P.; Williams, T. B.; Adhikari, S.; Dun, C.; Lu, C.; Itanze, D.; Jiang, L.; Carroll, D. L.; Donati, G. L.; Lundin, P. M.; Qiu, Y.; Geyer, S. M. Colloidal cobalt phosphide nanocrystals as trifunctional electrocatalysts for overall water splitting powered by a zinc–air battery. *Adv. Mater.* **2018**, *30*, 1705796. DOI:10.1002/adma.201705796

[25] Zou, W.; Dou, K.; Jiang, Q.; Xiang, J.; Kaun, C.-C.; Tang, H. Nearly spherical CoP nanoparticle/carbon nanosheet hybrids: A high-performance trifunctional electrocatalyst for oxygen reduction and water splitting. *RSC Adv.* **2019**, *9*, 39951–39957. DOI:10.1039/C9RA07334E

[26] Liu, H.; Guan, J.; Yang, S.; Yu, Y.; Shao, R.; Zhang, Z.; Dou, M.; Wang, F.; Xu, Q. Metal–organic framework-derived Co_2P nanoparticle/multi-doped porous carbon as a trifunctional electrocatalyst. *Adv. Mater.* **2020**, 2003649. DOI:10.1002/adma.202003649

[27] Shao, Q.; Li, Y.; Cui, X.; Li, T.; Wang, H.; Li, Y.; Duan, Q.; Si, Z. Metallophthalocyanine-based polymer-derived Co_2P nanoparticles anchoring on doped graphene as high-efficient trifunctional electrocatalyst for Zn–air batteries and water splitting. *ACS Sustain. Chem. Eng.* **2020**, *8*, 6422–6432. DOI:10.1021/acssuschemeng.0c00852

[28] Meng, T.; Hao, Y.-N.; Zheng, L.; Cao, M. Organophosphoric acid-derived CoP quantum dots@S,N-codoped graphite carbon as a trifunctional electrocatalyst for overall water splitting and Zn–air batteries. *Nanoscale* **2018**, *10*, 14613–14626. DOI:10.1039/C8NR03299H

[29] Guo, Y.; Yuan, P.; Zhang, J.; Xia, H.; Cheng, F.; Zhou, M.; Li, J.; Qiao, Y.; Mu, S.; Xu, Q.

Co_2P–CoN double active centers confined in N-doped carbon nanotube: Heterostructural engineering for trifunctional catalysis toward HER, ORR, OER, and Zn–air batteries driven water splitting. *Adv. Funct. Mater.* **2018**, *28*, 1805641. DOI:10.1002/adfm.201805641

[30] Zhang, Y.-Q.; Tao, H.-B.; Chen, Z.; Li, M.; Sun, Y.-F.; Hua, B.; Luo, J.-L. *In situ* grown cobalt phosphide (CoP) on perovskite nanofibers as an optimized trifunctional electrocatalyst for Zn–air batteries and overall water splitting. *J. Mater. Chem. A* **2019**, *7*, 26607–26617. DOI:10.1039/C9TA08936E

[31] Gao, L.; Zhu, M.; Zhang, Z.; Cui, G. Cobalt-boron-oxide supported on N,P dual-doped carbon nanosheets as the trifunctional electrocatalyst and its application in rechargeable Zn–air battery and overall water-electrolysis. *Electrochim. Acta* **2019**, *327*, 134980. DOI:10.1016/j.electacta.2019.134980

[32] Li, Y.; Cao, R.; Li, L.; Tang, X.; Chu, T.; Huang, B.; Yuan, K.; Chen, Y. Simultaneously integrating single atomic cobalt sites and Co_9S_8 nanoparticles into hollow carbon nanotubes as trifunctional electrocatalysts for Zn–air batteries to drive water splitting. *Small* **2020**, *16*, 1906735. DOI:10.1002/smll.201906735

[33] Wang, N.; Li, L.; Zhao, D.; Kang, X.; Tang, Z.; Chen, S. Graphene composites with cobalt sulfide: Efficient trifunctional electrocatalysts for oxygen reversible catalysis and hydrogen production in the same electrolyte. *Small* **2017**, *13*, 1701025. DOI:10.1002/smll.201701025

[34] Meng, T.; Qin, J.; Wang, S.; Zhao, D.; Mao, B.; Cao, M. *In situ* coupling of $Co_{0.85}Se$ and N-doped carbon via one-step selenization of metal–organic frameworks as a trifunctional catalyst for overall water splitting and Zn–air batteries. *J. Mater. Chem. A* **2017**, *5*, 7001–7014. DOI:10.1039/C7TA01453H

[35] Lyu, D.; Du, Y.; Huang, S.; Mollamahale, B. Y.; Zhang, X.; Hasan, S. W.; Yu, F.; Wang, S.; Tian, Z. Q.; Shen, P. K. Highly efficient multifunctional Co–N–C electrocatalysts with synergistic effects of Co–N moieties and Co metallic nanoparticles encapsulated in a N-doped carbon matrix for water-splitting and oxygen redox reactions. *ACS Appl. Mater. Interfaces* **2019**, *11*, 39809–39819. DOI:10.1021/acsami.9b11870

[36] Pei, Z.; Tang, Z.; Liu, Z.; Huang, Y.; Wang, Y.; Li, H.; Xue, Q.; Zhu, M.; Tang, D.; Zhi, C. Construction of a hierarchical 3D Co/N-carbon electrocatalyst for efficient oxygen reduction and overall water splitting. *J. Mater. Chem. A* **2018**, *6*, 489–497. DOI:10.1039/C7TA09254G

[37] Zhou, Z.; He, F.; Shen, Y.; Chen, X.; Yang, Y.; Liu, S.; Mori, T.; Zhang, Y. Coupling multiphase-Fe and hierarchical N-doped graphitic carbon as trifunctional electrocatalysts by supramolecular preorganization of precursors. *Chem. Commun.* **2017**, *53*, 2044–2047. DOI:10.1039/C6CC09442B

[38] Qin, Q.; Jang, H.; Li, P.; Yuan, B.; Liu, X.; Cho, J. A tannic acid–derived N,P-codoped carbon-supported iron-based nanocomposite as an advanced trifunctional electrocatalyst for the overall water splitting cells and zinc–air batteries. *Adv. Energy Mater.* **2019**, *9*, 1803312. DOI:10.1002/aenm.201803312

[39] Yang, J.; Wang, X.; Li, B.; Ma, L.; Shi, L.; Xiong, Y.; Xu, H. Novel iron/cobalt-containing polypyrrole hydrogel-derived trifunctional electrocatalyst for self-powered overall water splitting. *Adv. Funct. Mater.* **2017**, *27*, 1606497. DOI:10.1002/adfm.201606497

[40] Kong, F.; Fan, X.; Kong, A.; Zhou, Z.; Zhang, X.; Shan, Y. Covalent phenanthroline framework derived FeS@Fe_3C composite nanoparticles embedding in N-S-codoped carbons as highly efficient trifunctional electrocatalysts. *Adv. Funct. Mater.* **2018**, *28*, 1803973. DOI:10.1002/adfm.201803973

[41] Devi, B.; Koner, R. R.; Halder, A. Ni(II)-dimeric complex-derived nitrogen-doped graphitized carbon-encapsulated nickel nanoparticles: Efficient trifunctional electrocatalyst for oxygen reduction reaction, oxygen evolution reaction, and hydrogen evolution reaction. *ACS Sustain. Chem. Eng.* **2019**, *7*, 2187–2199. DOI:10.1021/acssuschemeng.8b04883

[42] Diao, J.; Qiu, Y.; Liu, S.; Wang, W.; Chen, K.; Li, H.; Yuan, W.; Qu, Y.; Guo, X. Interfacial engineering of W_2N/WC heterostructures derived from solid-state synthesis: A highly efficient trifunctional electrocatalyst for ORR, OER, and HER. *Adv. Mater.* **2020**, *32*, 1905679. DOI:10.1002/adma.201905679

[43] Peng, X.; Zhao, S.; Mi, Y.; Han, L.; Liu, X; Qi, D.; Sun, J.; Liu, Y.; Bao, H.; Zhuo, L.; Xin, H. L.; Luo, J.; Sun, X. Trifunctional single-atomic Ru sites enable efficient overall water splitting and oxygen reduction in acidic media. *Small* **2020**, 2002888. DOI:10.1002/smll.202002888

[44] Tang, C.; Zhong, L.; Zhang, B.; Wang, H.-F.; Zhang, Q. 3D mesoporous van der waals heterostructures for trifunctional energy electrocatalysis. *Adv. Mater.* **2018**, *30*, 1705110. DOI:10.1002/adma.201705110

[45] He, L.; Liu, J.; Hu, B. ; Liu, Y.; Cui, B.; Peng, D.; Zhang, Z.; Wu, S.; Liu, B. Cobalt oxide doped with titanium dioxide and embedded with carbon nanotubes and graphene-like nanosheets for efficient trifunctional electrocatalyst of hydrogen evolution, oxygen reduction, and oxygen evolution reaction. *J. Power Sources* **2019**, *414*, 333–344. DOI:10.1016/j.jpowsour.2019.01.020

[46] Alshehri, S. M.; Alhabarah, A. N.; Ahmed, J.; Naushad, M.; Ahamad, T. An efficient and cost-effective tri-functional electrocatalyst based on cobalt ferrite embedded nitrogen doped carbon. *J. Colloid Interface Sci.* **2018**, *514*, 1–9. DOI:10.1016/j.jcis.2017.12.020

[47] Kwak, I.; Kwon, I. S.; Kim, J.; Park, K.; Ahn, J.-P.; Yoo, S. J.; Kim, J.-G.; Park, J. IrO_2–ZnO hybrid nanoparticles as highly efficient trifunctional electrocatalysts. *J. Phys. Chem. C* **2017**, *121*, 14899–14906. DOI:10.1021/acs.jpcc.7b03844

[48] Deng, C.; Wu, K.-H.; Scott, J.; Zhu, S.; Zheng, X.; Amal, R.; Wang, D.-W. Spherical Murray-type assembly of Co–N–C nanoparticles as a high-performance trifunctional electrocatalyst. *ACS Appl. Mater. Interfaces* **2019**, *11*, 9925–9933. DOI:10.1021/acsami.8b20565

[49] Li, K.; Guo, D.; Kang, J.; Wei, B.; Zhang, X.; Chen, Y. Hierarchical hollow spheres assembled with ultrathin CoMn double hydroxide nanosheets as trifunctional electrocatalyst for overall water splitting and Zn air battery. *ACS Sustain. Chem. Eng.* **2018**, *6*, 14641–14651. DOI:10.1021/acssuschemeng.8b03232

[50] Sun, T.; Zhang, S.; Xu, L.; Wang, D.; Li, Y. An efficient multifunctional hybrid electrocatalyst: Ni_2P nanoparticles on MOF-derived Co,N-doped porous carbon polyhedrons for oxygen reduction and water splitting. *Chem. Commun.* **2018**, *54*, 12101–12104. DOI:10.1039/C8CC06566G

[51] Surendran, S.; Shanmugapriya, S.; Sivanantham, A.; Shanmugam, S.; Selvan, R. K. Electrospun carbon nanofibers encapsulated with nicop: a multifunctional electrode for supercapattery and oxygen reduction, oxygen evolution, and hydrogen evolution reactions. *Adv. Energy Mater.* **2018**, *8*, 1800555. DOI:10.1002/aenm.201800555

[52] Ren, J.-T.; Chen, L.; Wang, Y.-S.; Tian, W.-W.; Gao, L.-J.; Yuan, Z.-Y. FeNi nanoalloys encapsulated in N-doped CNTs tangled with N-doped carbon nanosheets as efficient multifunctional catalysts for overall water splitting and rechargeable Zn–air batteries. *ACS Sustain. Chem. Eng.* **2020**, *8*, 223–237. DOI:10.1021/acssuschemeng.9b05238

[53] Bian, Y. ; Wang, H.; Gao, Z.; Hu, J.; Liu, D.; Dai, L. A facile approach to high-performance trifunctional electrocatalysts by substrate-enhanced electroless deposition of Pt/NiO/Ni on carbon nanotubes. *Nanoscale* **2020**, *12*, 14615–14625. DOI:10.1039/D0NR03378B

[54] Lv, X.; Tian, W.; Liu, Y.; Yuan, Z.-Y. Well-defined CoP/Ni_2P nanohybrids encapsulated in a nitrogen-doped carbon matrix as advanced multifunctional electrocatalysts for efficient overall water splitting and zinc–air batteries. *Mater. Chem. Front.* **2019**, *3*, 2428–2436. DOI:10.1039/C9QM00449A

[55] Bai, Z.; Li, S.; Fu, J.; Zhang, Q.; Chang, F.; Yang, L.; Lu, J.; Chen, Z. Metal-organic framework-derived nickel cobalt oxysulfide nanocages as trifunctional electrocatalysts for high efficiency power to hydrogen. *Nano Energy* **2019**, *58*, 680–686. DOI:10.1016/j.nanoen.2019.01.050

[56] Shi, Q.; Liu, Q.; Ma, Y.; Fang, Z.; Liang, Z.; Shao, G.; Tang, B.; Yang, W.; Qin, L.; Fang, X. High-performance trifunctional electrocatalysts based on FeCo/Co_2P hybrid nanoparticles for zinc–air battery and self-powered overall water splitting. *Adv. Energy Mater.* **2020**, *10*, 1903854. DOI:10.1002/aenm.201903854

[57] Zhang, W.; Zhao, J.; Zhang, J.; Chen, X.; Zhang, X.; Yang, F. Electronic asymmetric distribution of RhCu bimetallic nanocrystals for enhancing trifunctional electrocatalysis. *ACS Appl. Mater. Interfaces* **2020**, *12*, 10299–10306. DOI:10.1021/acsami.9b19980

[58] Bai, J.; Meng, T.; Guo, D.; Wang, S.; Mao, B.; Cao, M. Co_9S_8@MoS_2 core–shell heterostructures as trifunctional electrocatalysts for overall water splitting and Zn–air batteries. *ACS Appl. Mater. Interfaces* **2018**, *10*, 1678–1689. DOI:10.1021/acsami.7b14997

[59] Prabhakaran, S.; Balamurugan, J.; Kim, N. H.; Lee, J. H. Hierarchical 3D oxygenated cobalt molybdenum selenide nanosheets as robust trifunctional catalyst for water splitting and zinc–air batteries. *Small* **2020**, *16*, 2000797. DOI:10.1002/smll.202000797

[60] Zhang, W.; Zhao, X.; Zhao, Y.; Zhang, J.; Li, X.; Fang, L.; Li, L. Mo-doped Zn, Co zeolitic imidazolate framework-derived Co_9S_8 quantum dots and MoS_2 embedded in three-dimensional nitrogen-doped carbon nanoflake arrays as an efficient trifunctional electrocatalysts for the oxygen reduction reaction, oxygen evolution reaction, and hydrogen evolution reaction. *ACS Appl. Mater. Interfaces* **2020**, *12*, 10280–10290. DOI:10.1021/acsami.9b19193

[61] Kong, F.; Zhang, C.; Qiao, Y.; Li, R.; Kong, A.; Shan, Y. Coupled nanocomposite $Co_{5.47}N$–Co_3Fe_7 inlaid in a tremella-like carbon framework as a highly efficient multifunctional electrocatalyst for oxygen transformation and overall water splitting. *Sustain. Energy Fuels* **2019**, *3*, 3538–3549. DOI:10.1039/C9SE00657E

[62] Sun, H.; Li, Q.; Lian, Y.; Zhang, C.; Qi, P.; Mu, Q.; Jin, H.; Zhang, B.; Chen, M.; Deng, Z.; Peng, Y. Highly efficient water splitting driven by zinc–air batteries with a single catalyst incorporating rich active species. *Appl. Catal. B Environ.* **2020**, *263*, 118139. DOI:10.1016/j.apcatb.2019.118139

[63] Yang, C. C.; Zai, S. F.; Zhou, Y. T.; Du, L.; Jiang, Q. Fe_3C–Co nanoparticles encapsulated in a hierarchical structure of N-doped carbon as a multifunctional electrocatalyst for ORR, OER, and HER. *Adv. Funct. Mater.* **2019**, 1901949. DOI:10.1002/adfm.201901949

[64] Hu, C.; Dai, L. Multifunctional carbon-based metal-free electrocatalysts for simultaneous oxygen reduction, oxygen evolution, and hydrogen evolution. *Adv. Mater.* **2017**, *29*, 1604942. DOI:10.1002/adma.201604942

[65] Hu, Q.; Li, G.; Li, G.; Liu, X.; Zhu, B.; Chai, X.; Zhang, Q.; Liu, J.; He, C. Trifunctional electrocatalysis on dual-doped graphene nanorings–integrated boxes for efficient water

splitting and Zn–air batteries. *Adv. Energy Mater.* **2019**, *9*, 1803867. DOI:10.1002/aenm.201803867

[66] Jia, Y.; Zhang, L.; Du, A.; Gao, G.; Chen, J.; Yan, X.; Brown, C. L.; Yao, X. Defect graphene as a trifunctional catalyst for electrochemical reactions. *Adv. Mater.* **2016**, *28*, 9532. DOI:10.1002/adma.201602912

[67] Jiang, H.; Gu, J.; Zheng, X.; Liu, M.; Qiu, X.; Wang, L.; Li, W.; Chen, Z.; Ji, X.; Li, J. Defect-rich and ultrathin N doped carbon nanosheets as advanced trifunctional metal-free electrocatalysts for the ORR, OER and HER. *Energy Environ. Sci.* **2019**, *12*, 322–333. DOI:10.1039/C8EE03276A

[68] Hang, C.; Zhang, J.; Zhu, J.; Li, W.; Kou, Z.; Huang, Y. In situ exfoliating and generating active sites on graphene nanosheets strongly coupled with carbon fiber toward self-standing bifunctional cathode for rechargeable Zn–air batteries. *Adv. Energy Mater*. **2018**, *8*, 1703539. DOI:10.1002/aenm.201703539

NMR Spectra

Benzoic acid

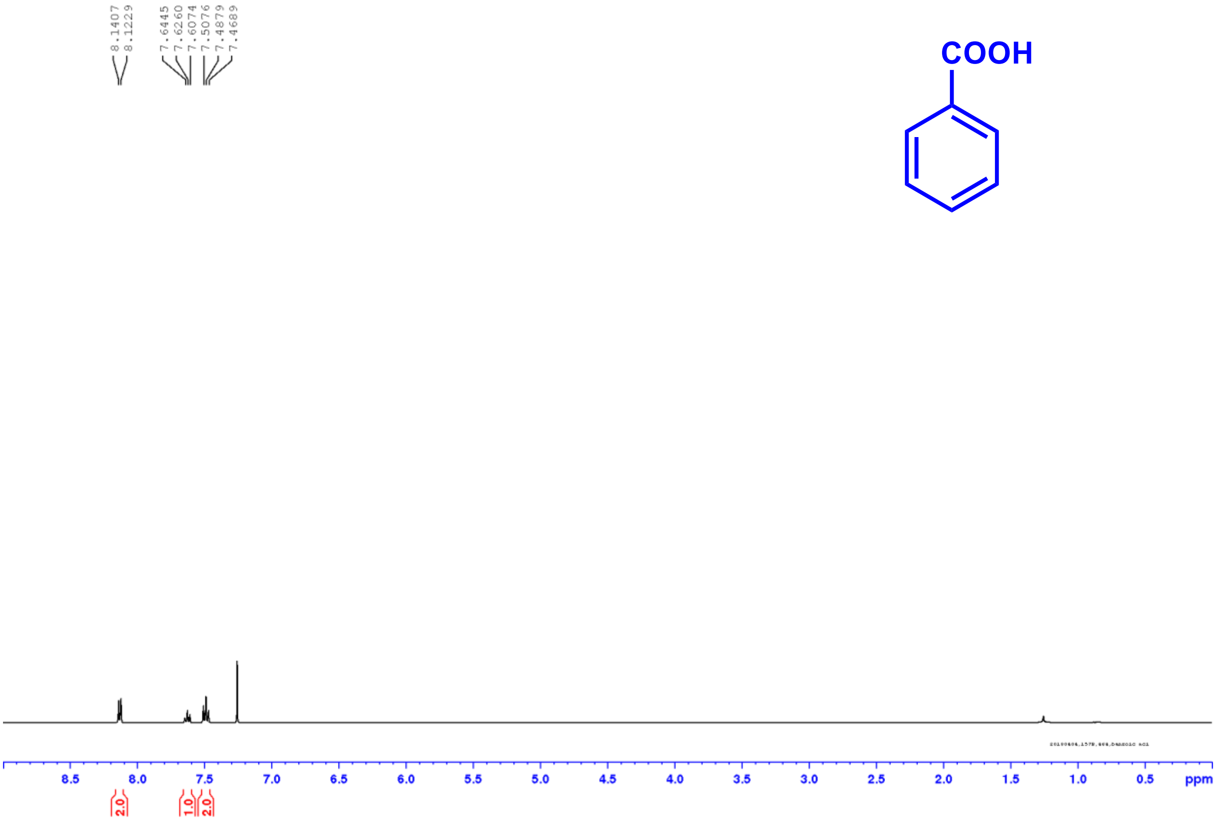

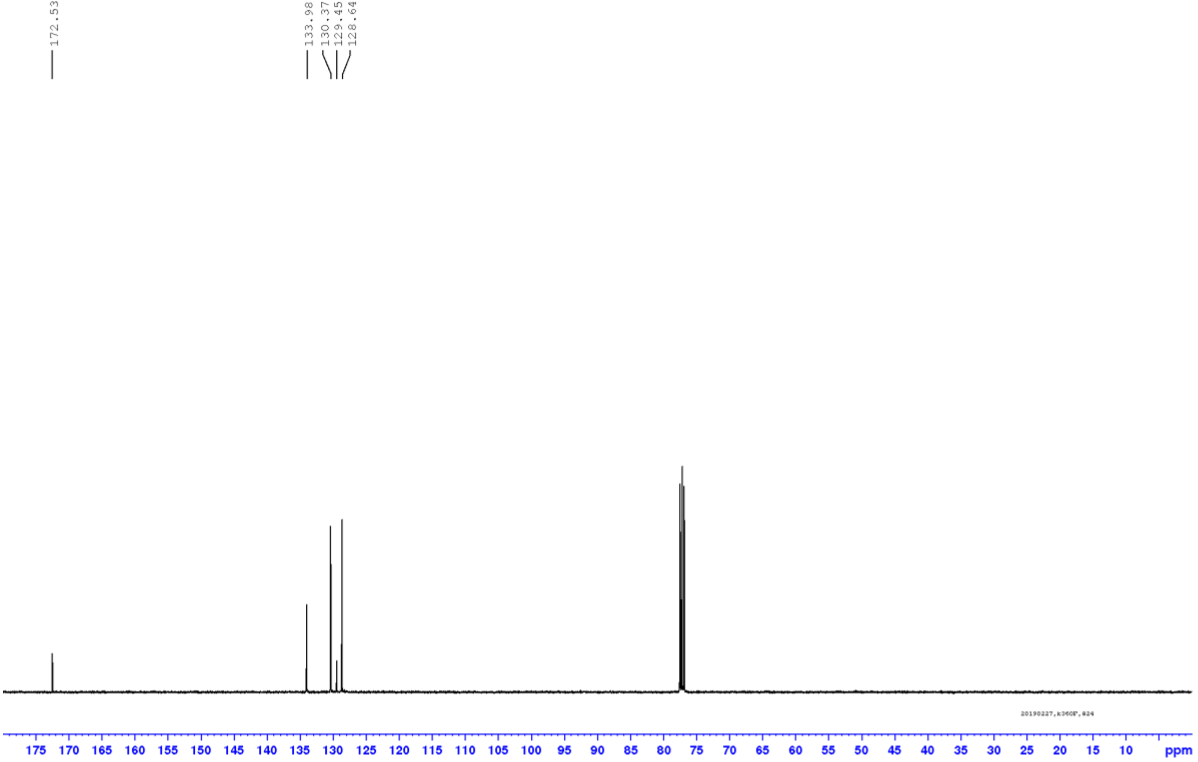

Acetophenone

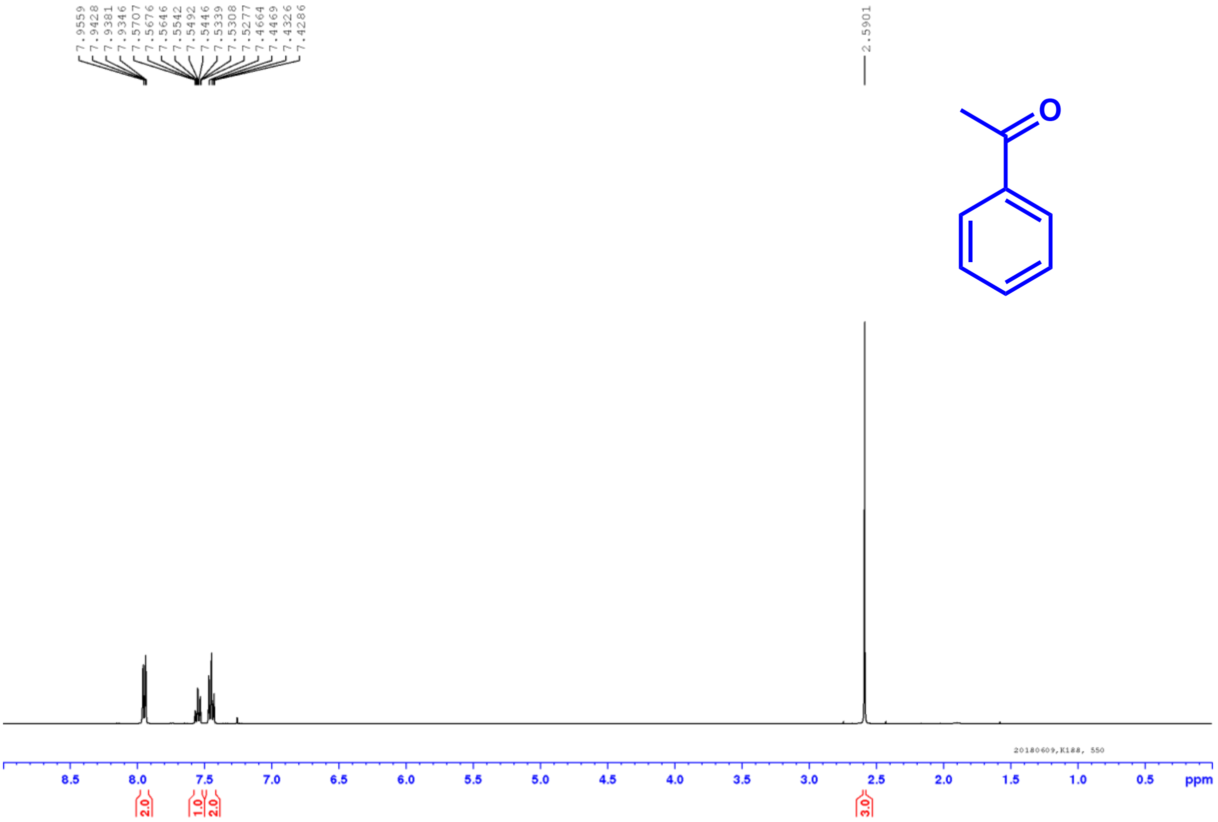

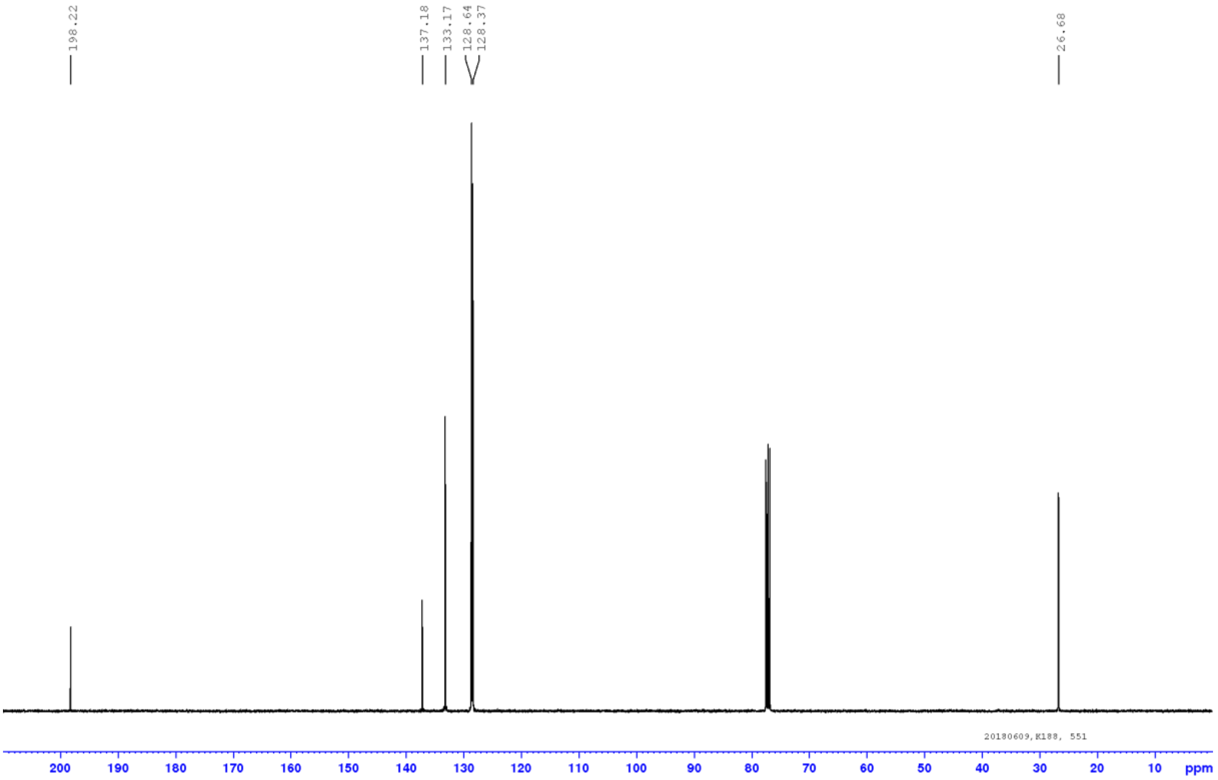

Benzophenone

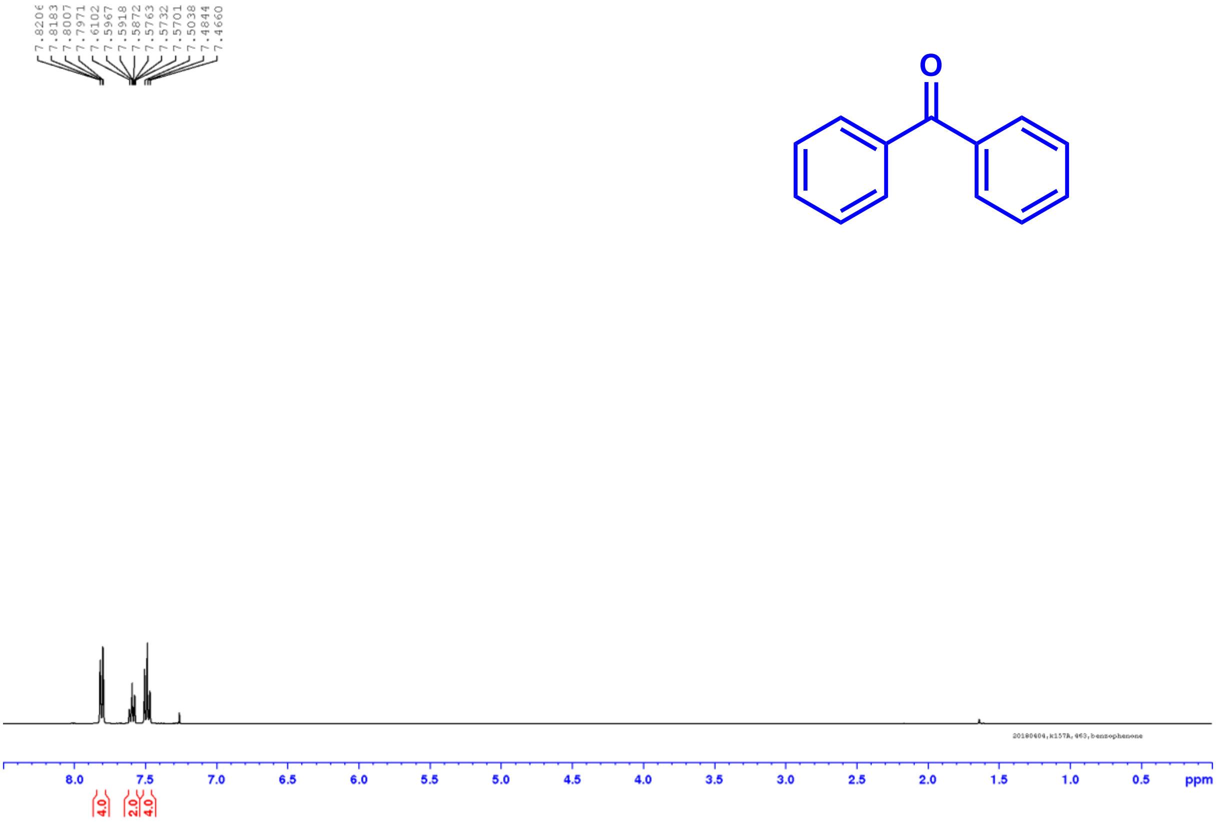

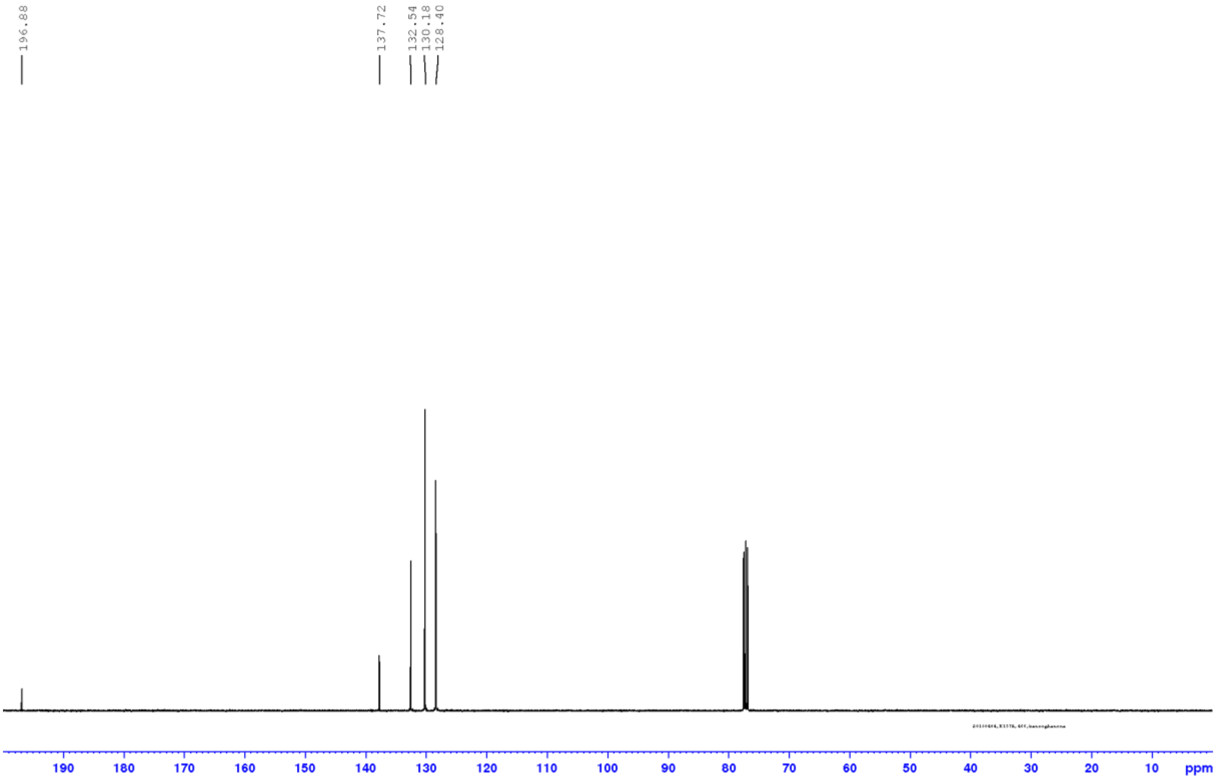

4-Methylbenzoic acid

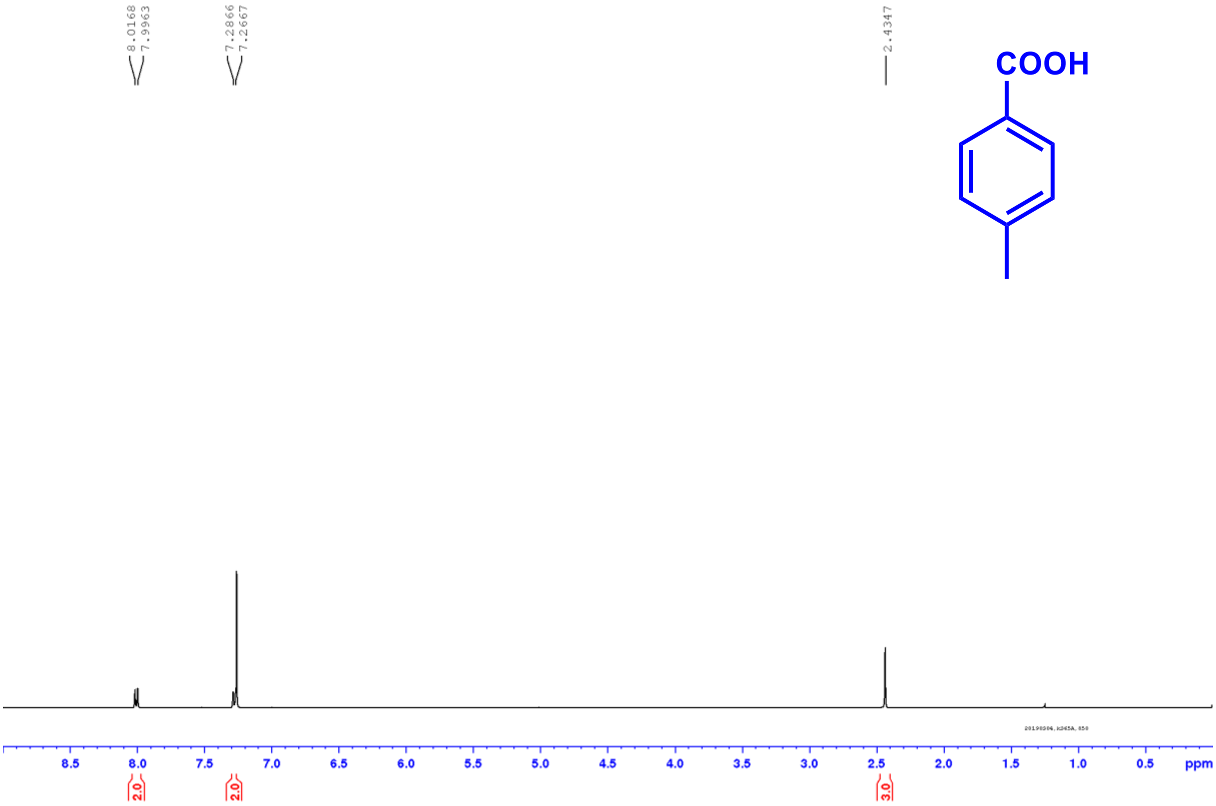

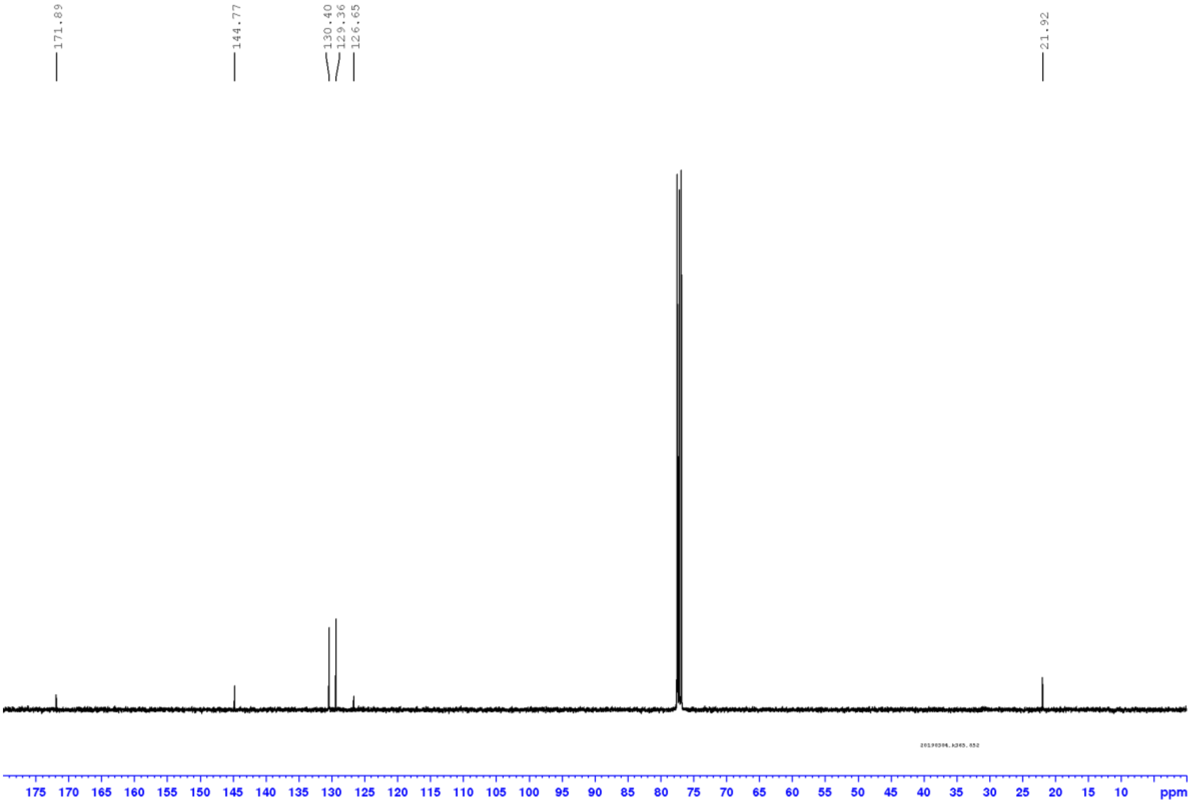

Terephthalic acid

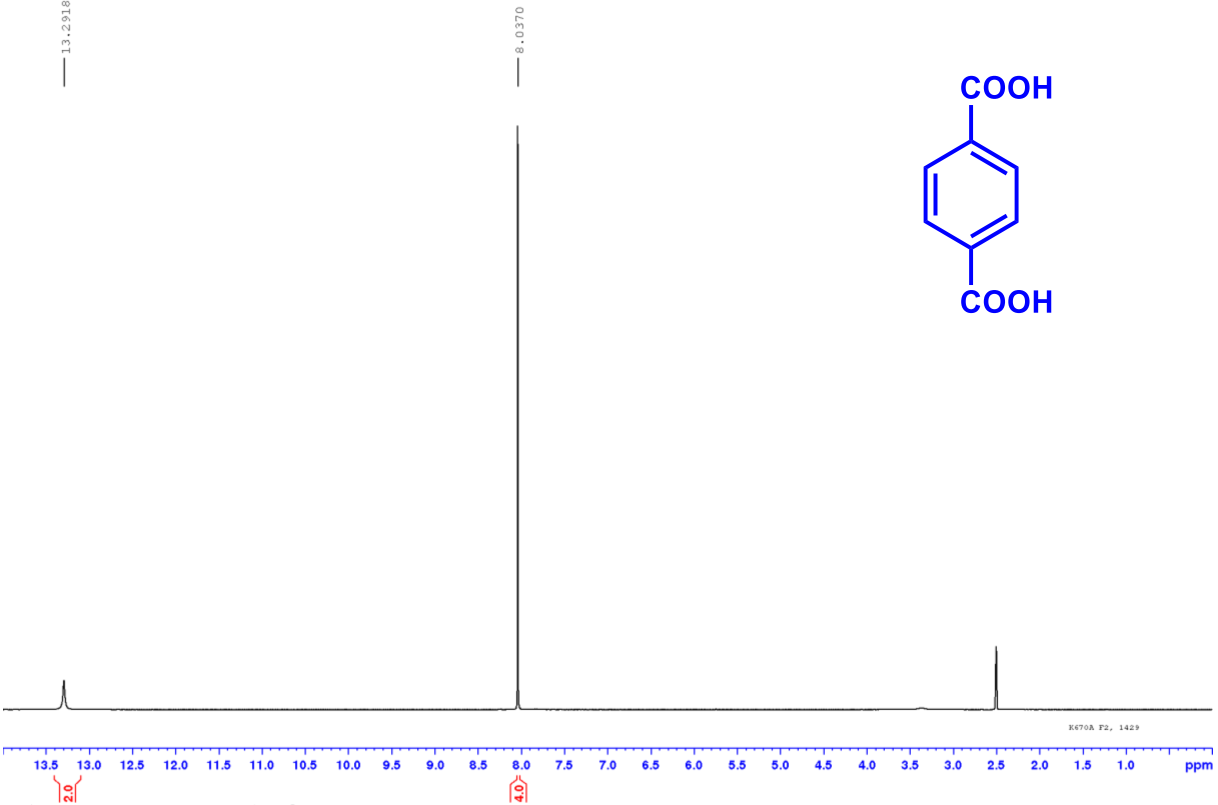

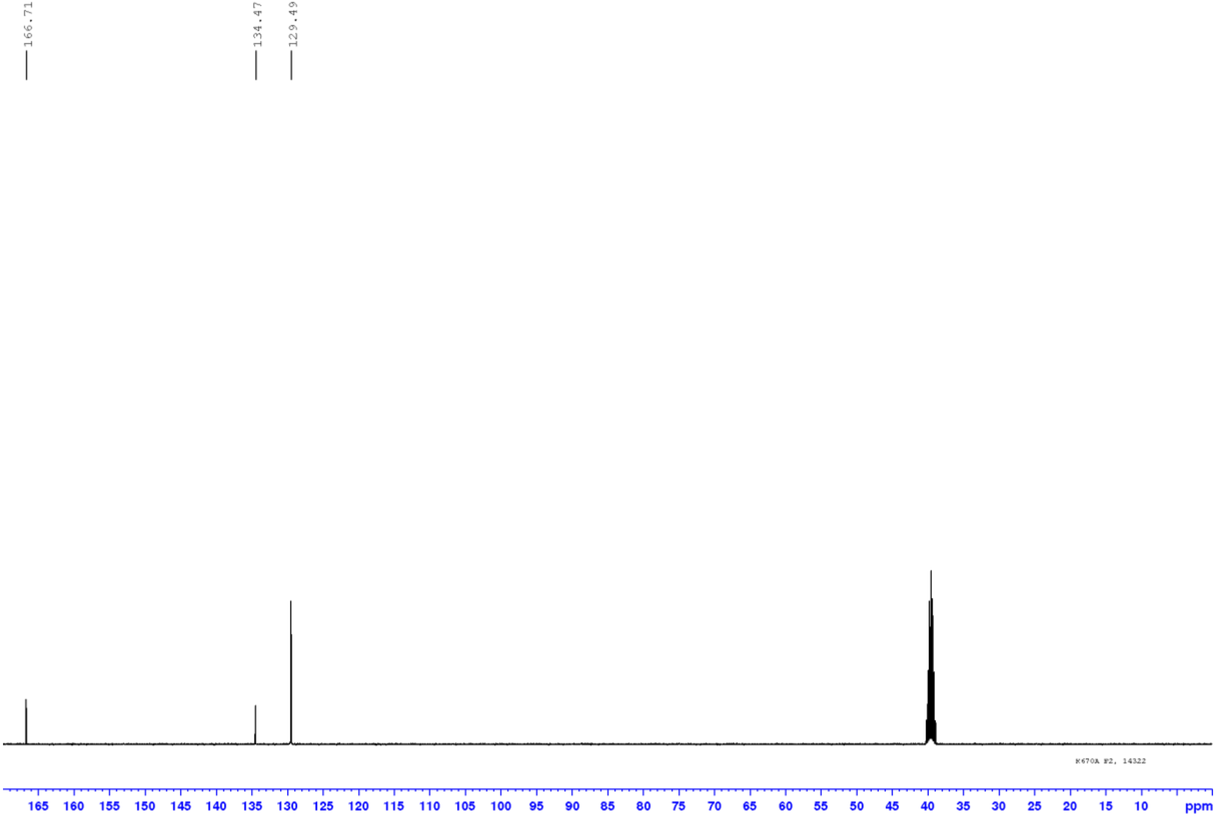

3-Methylbenzoic acid

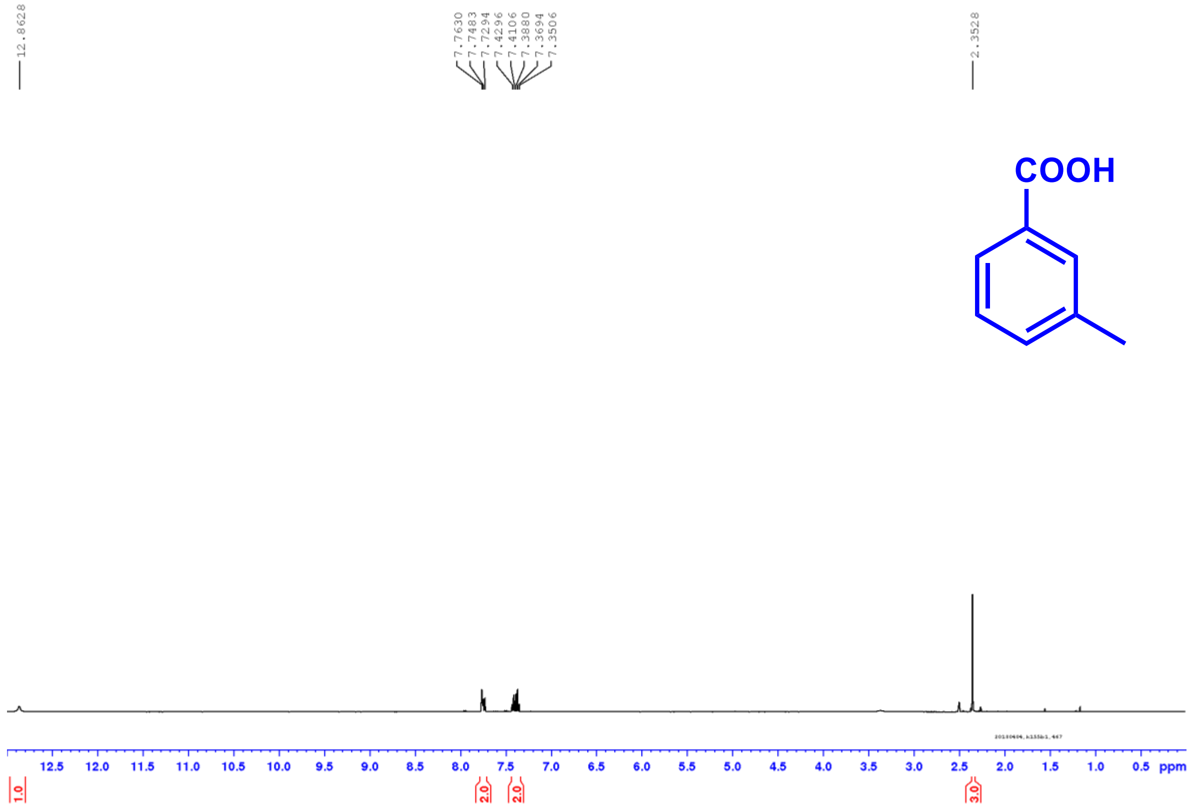

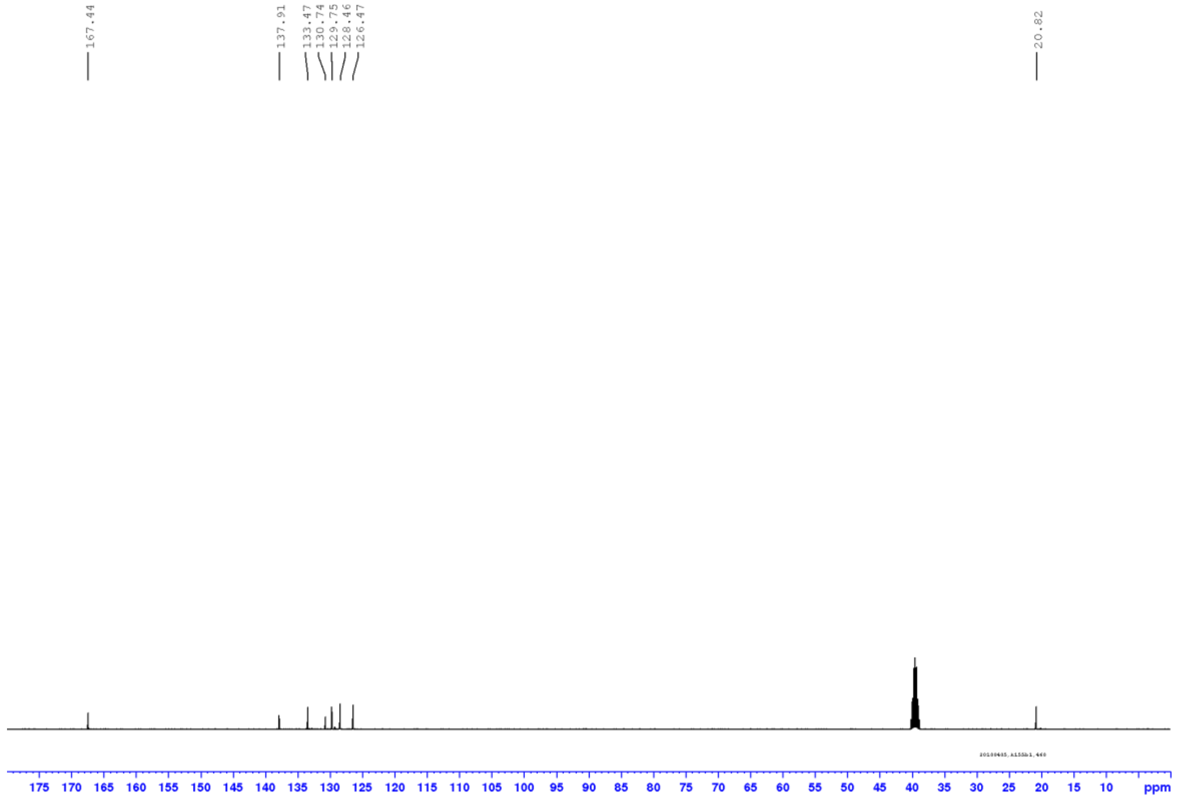

Isophthalic acid

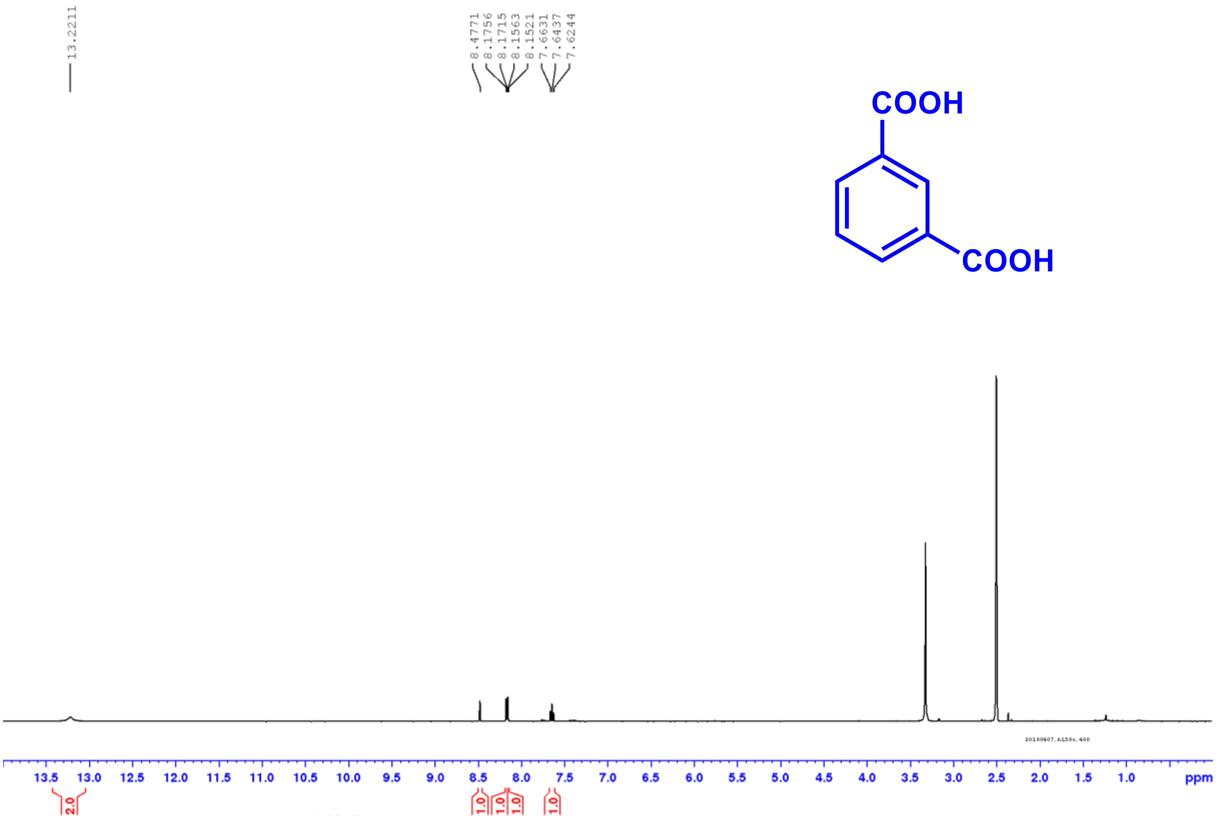

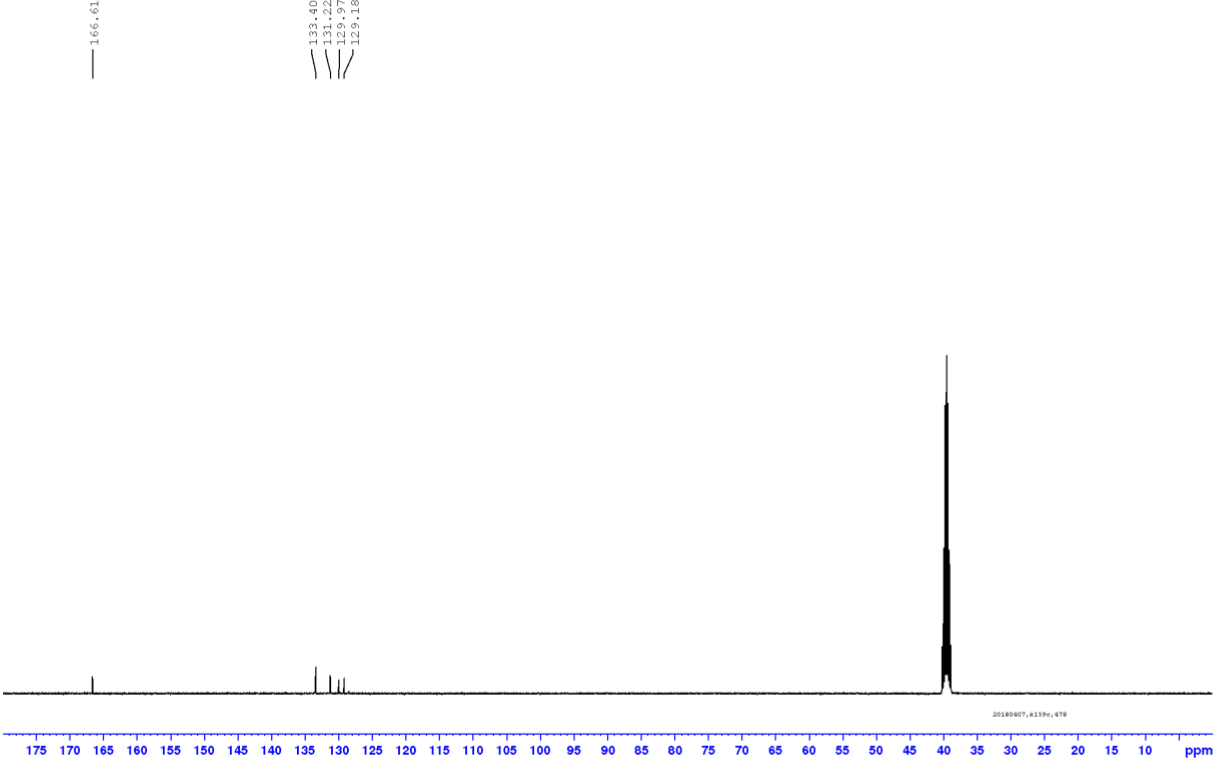

3,5-Dimethylbenzoic acid

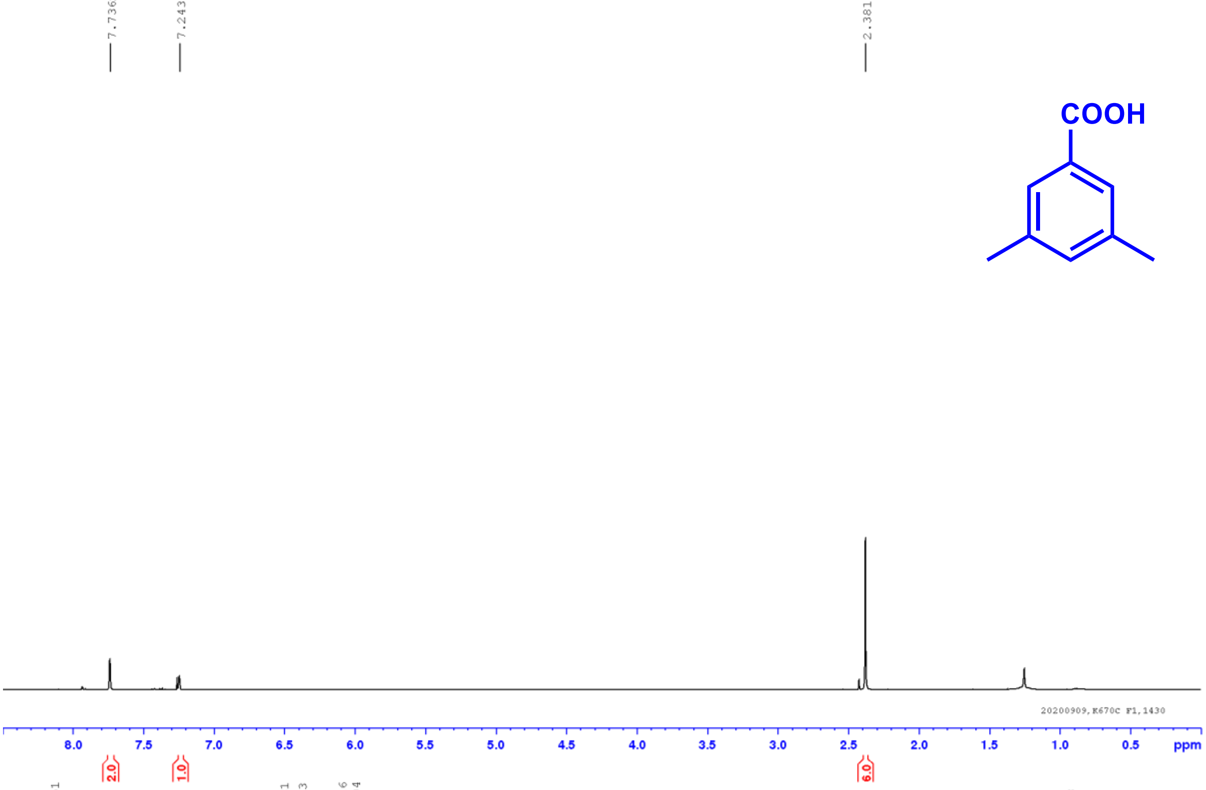

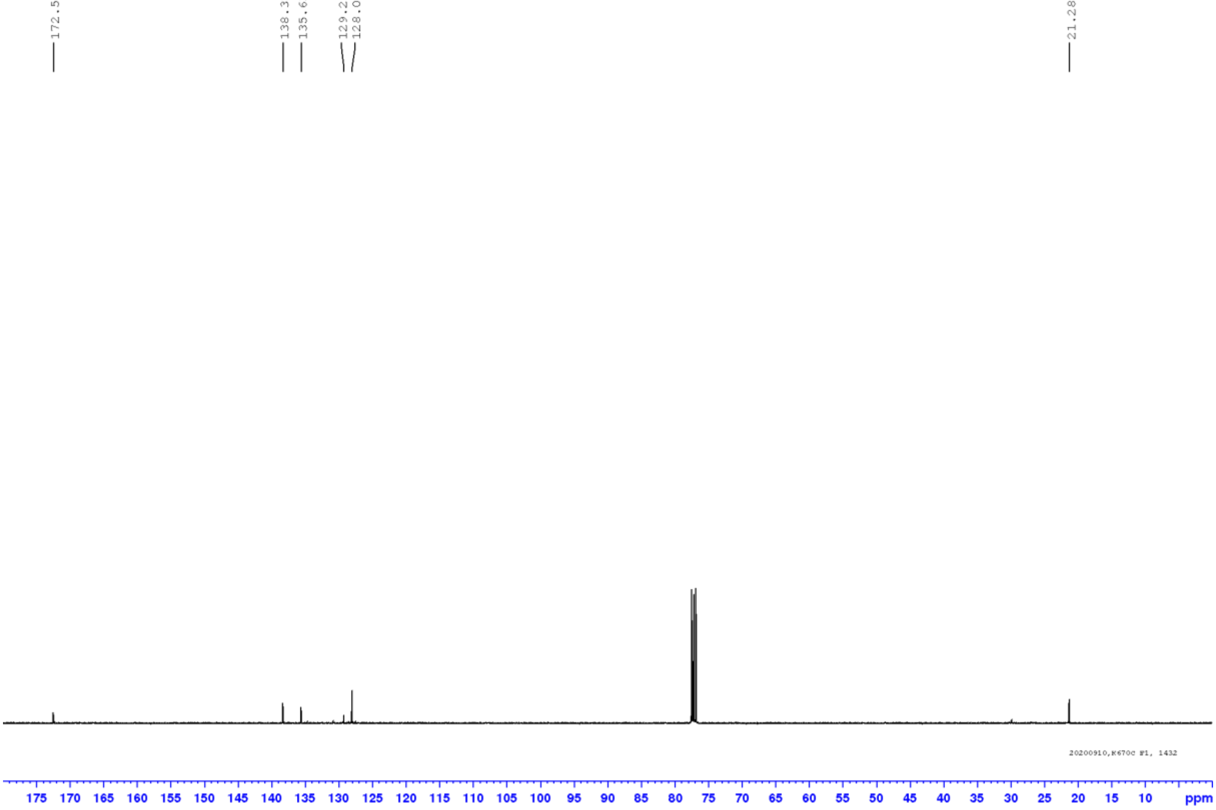

5-Methylisophthalic acid

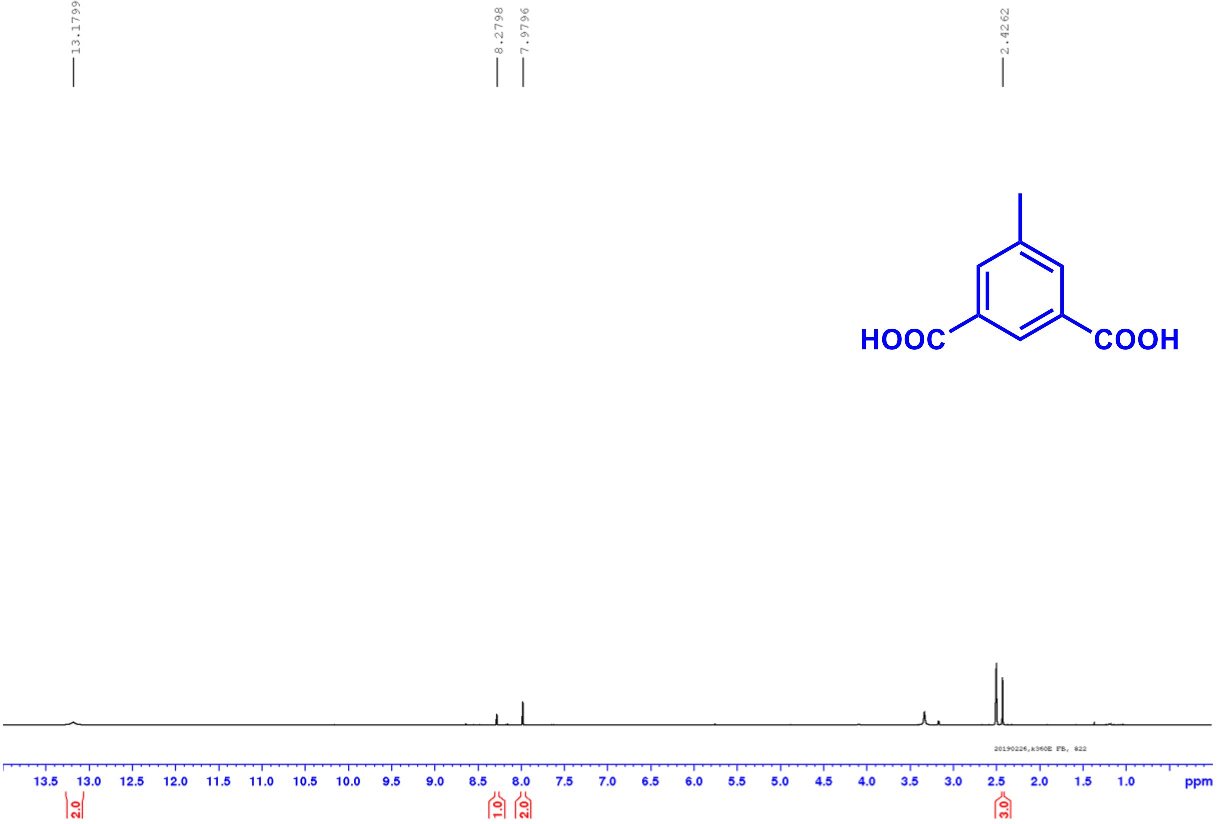

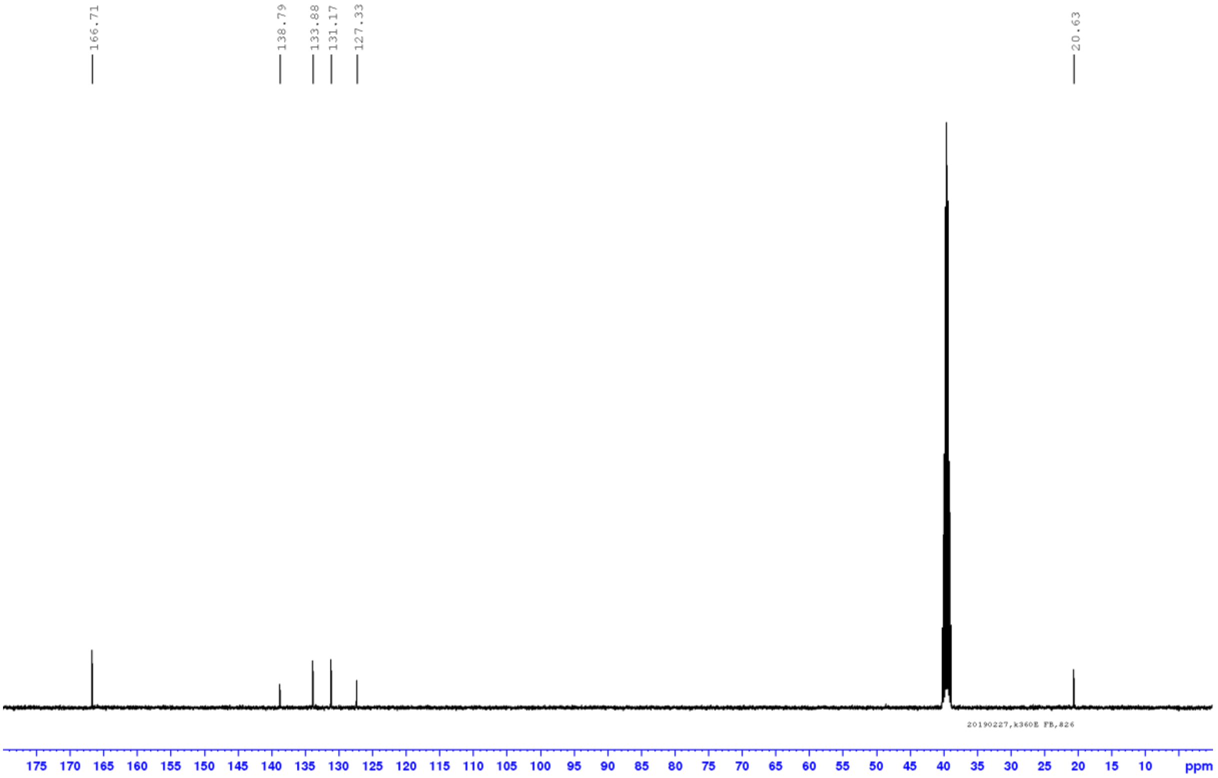

1,2-Diphenylethane

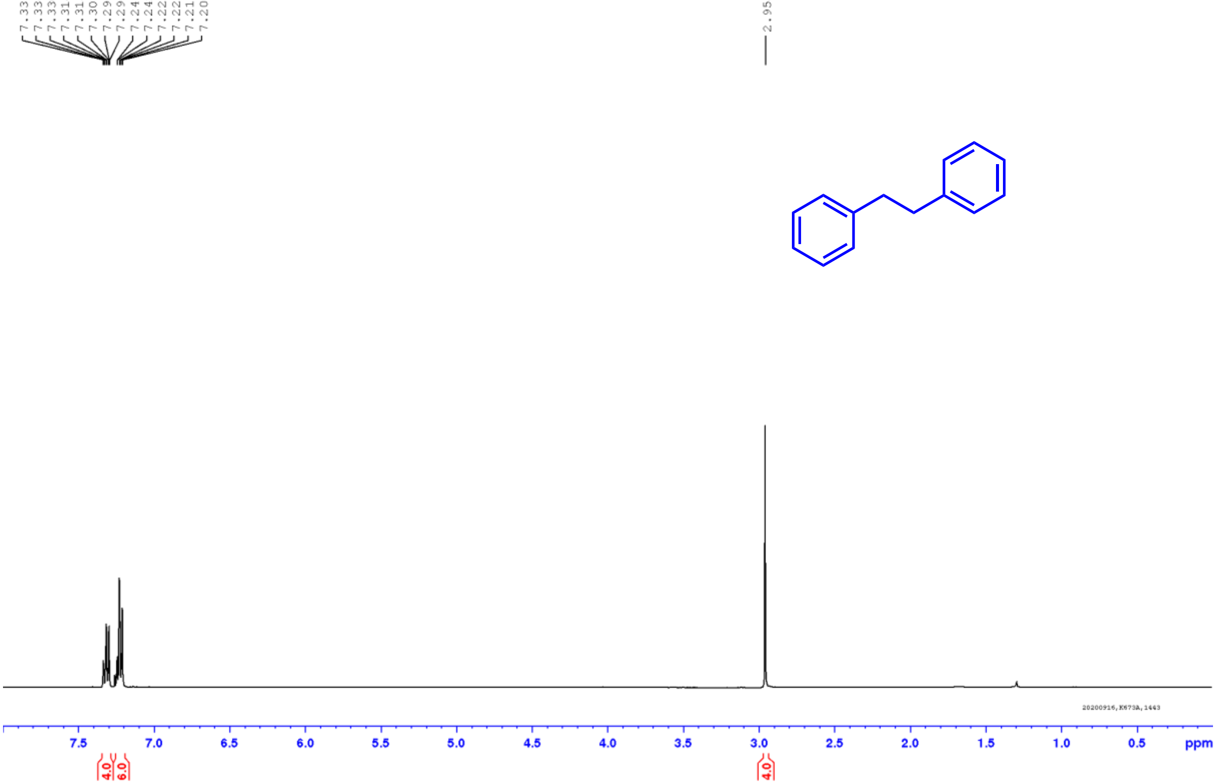

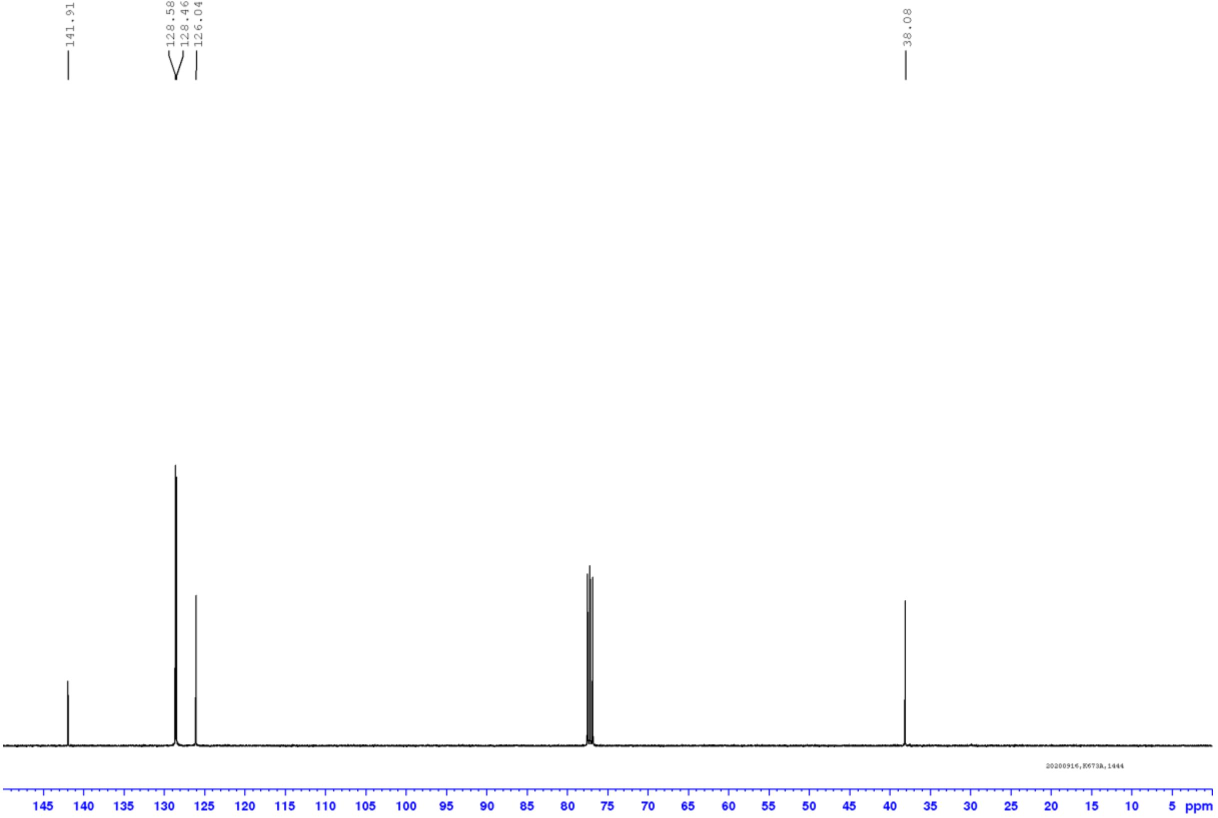

1,2-Bis(4-bromophenyl)ethane

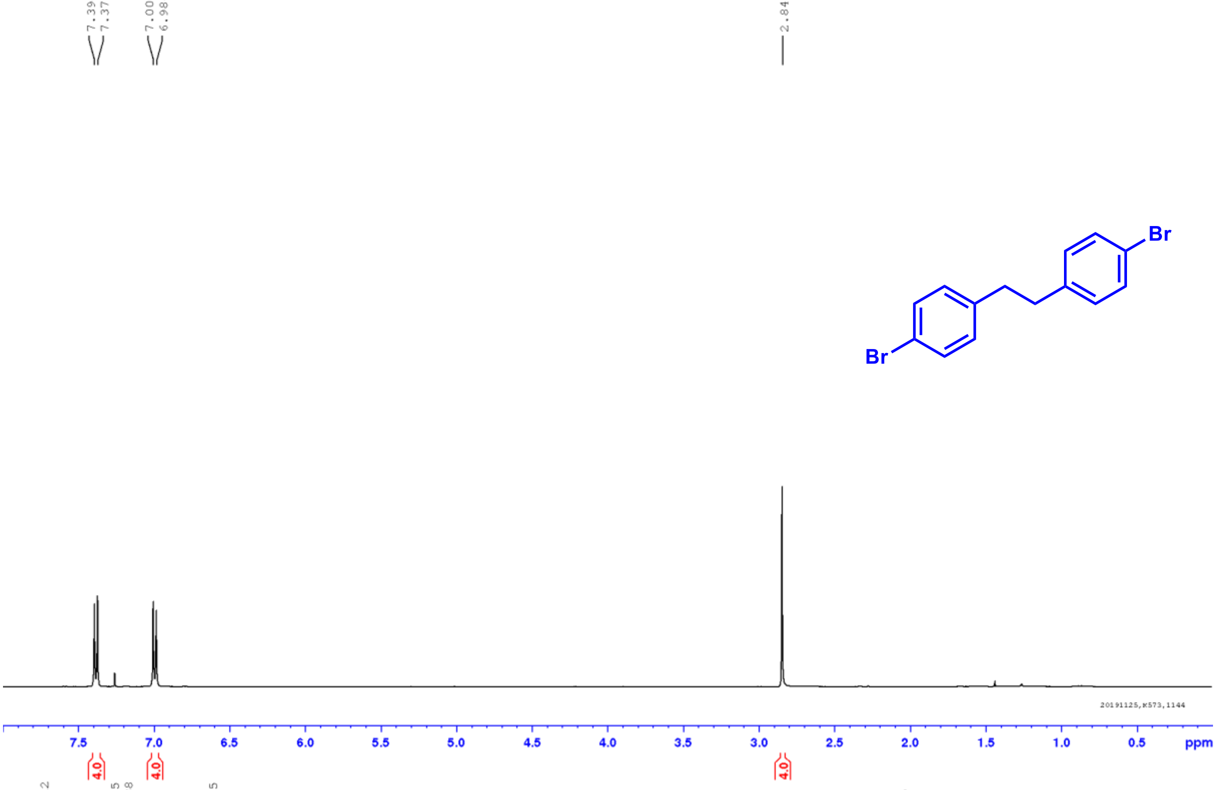

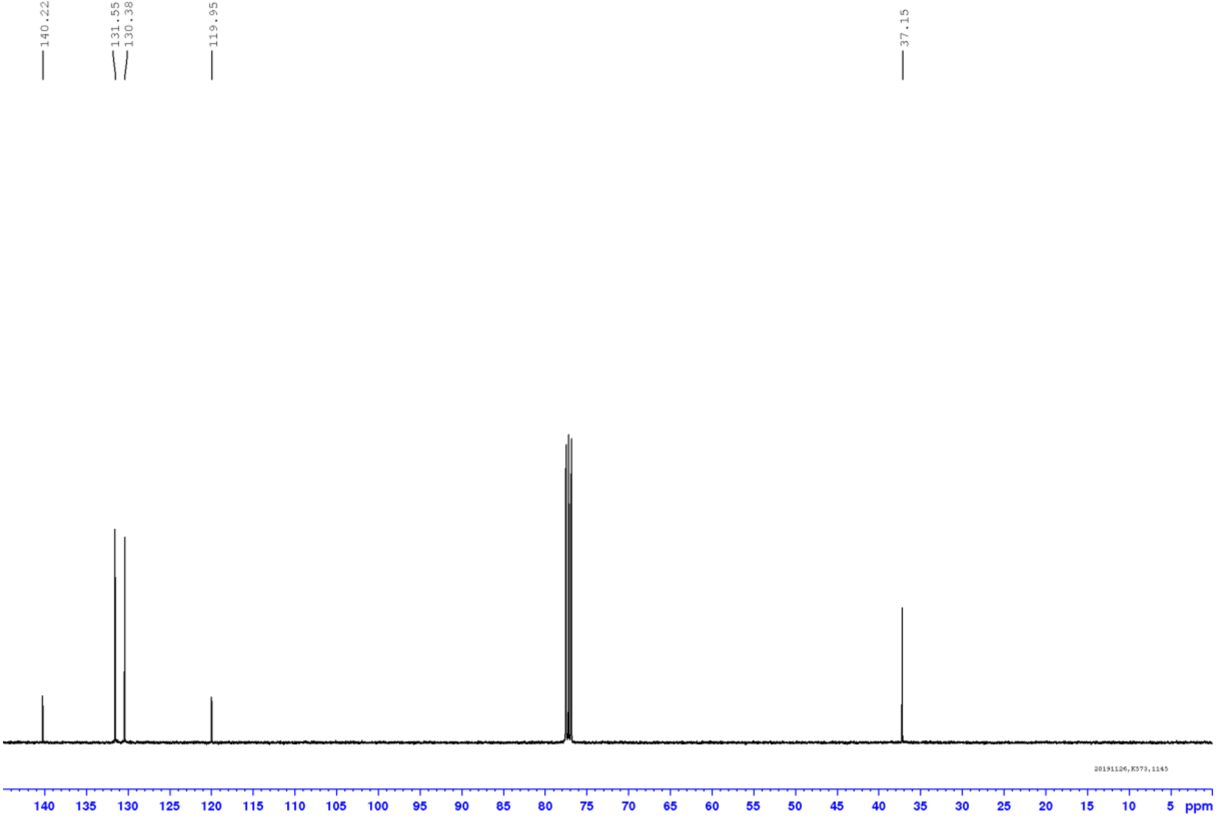

1,2-Bis(4-iodophenyl)ethane

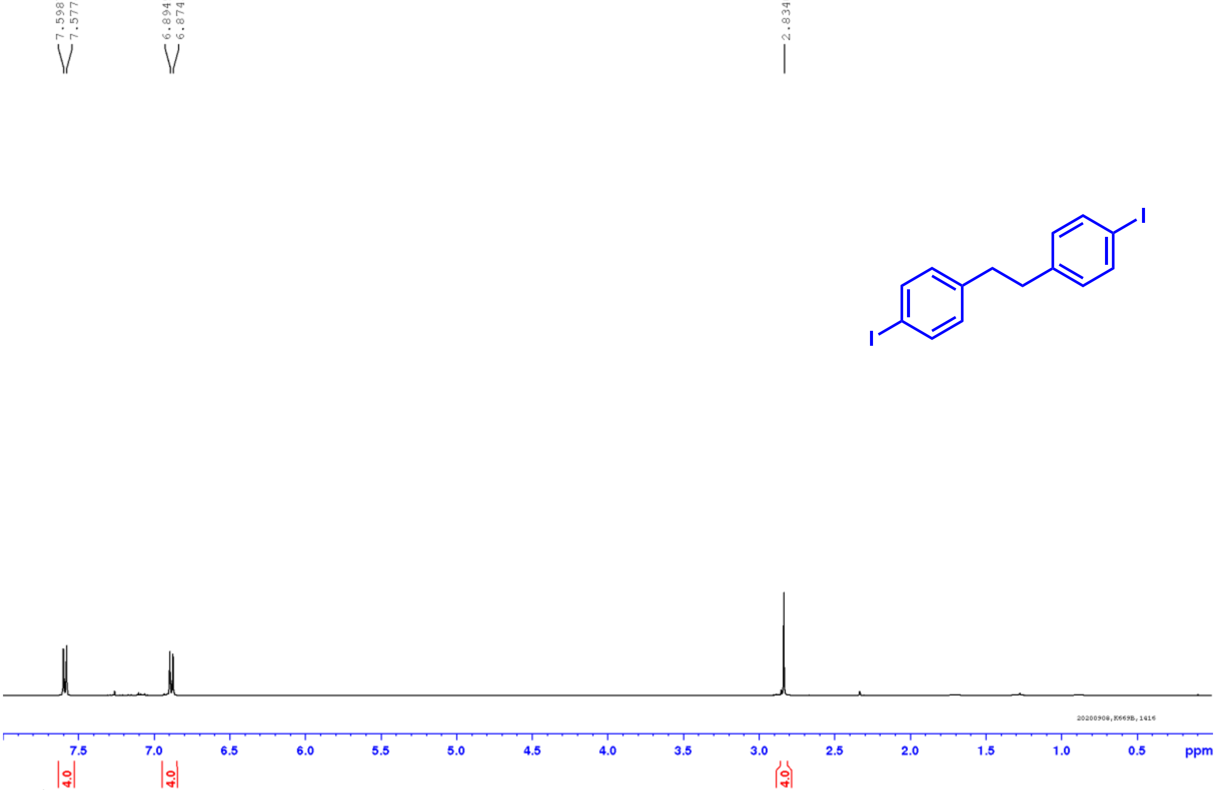

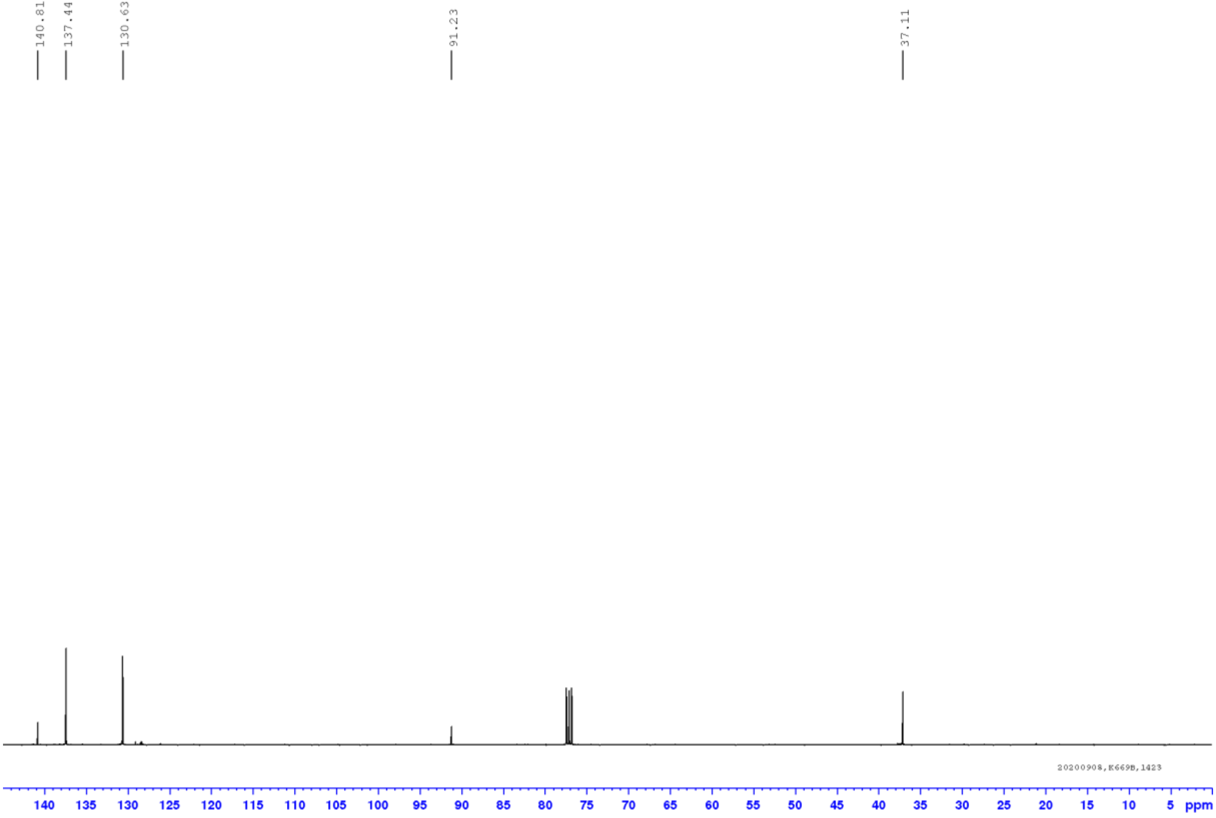

1,2-Di-*p*-tolylethane

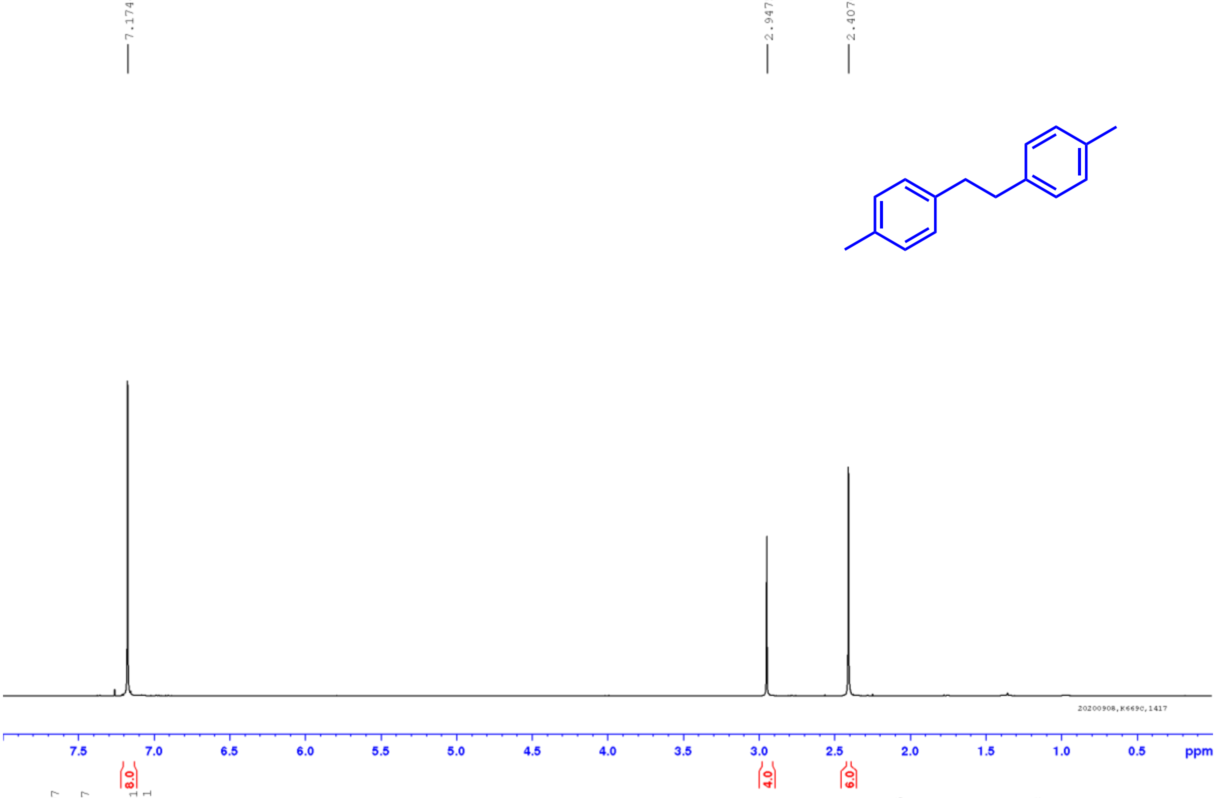

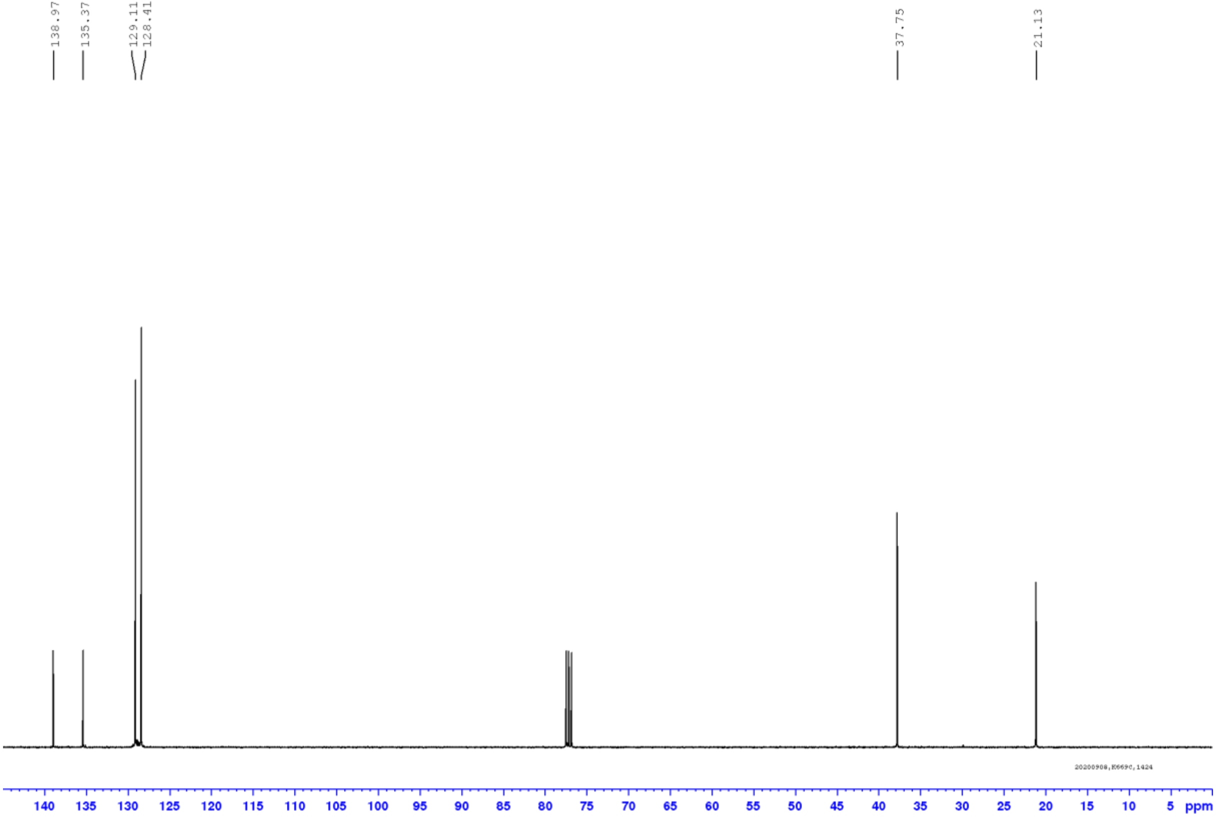

1,2-Bis(2-fluorophenyl)ethane

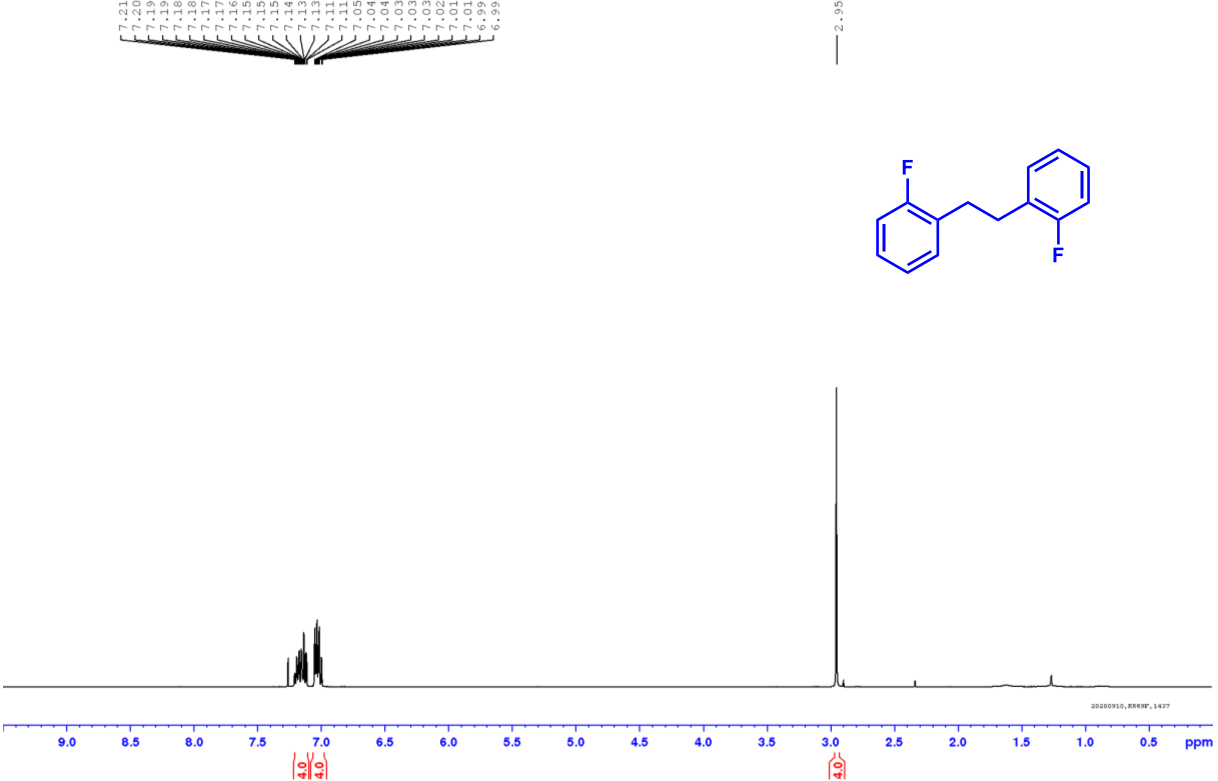

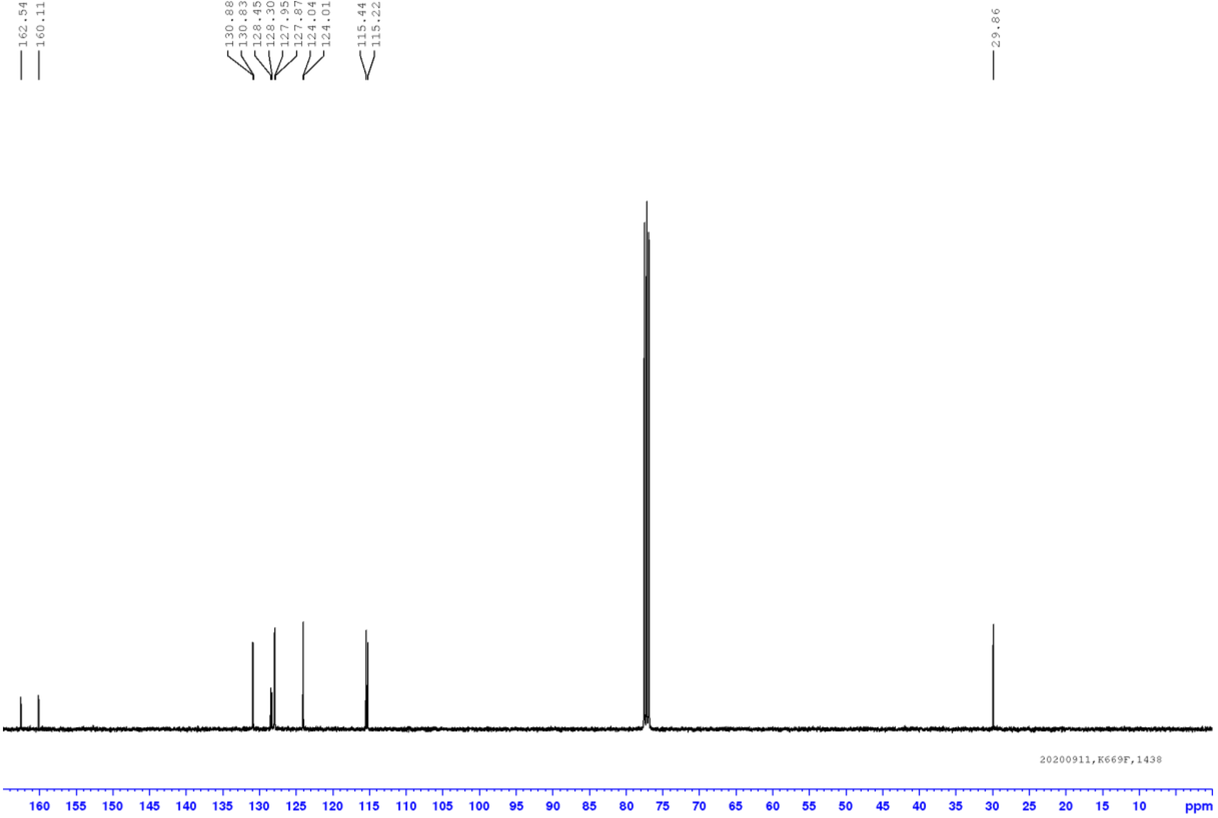

1,2-Bis(2-fluorophenyl)ethane

^{19}F NMR

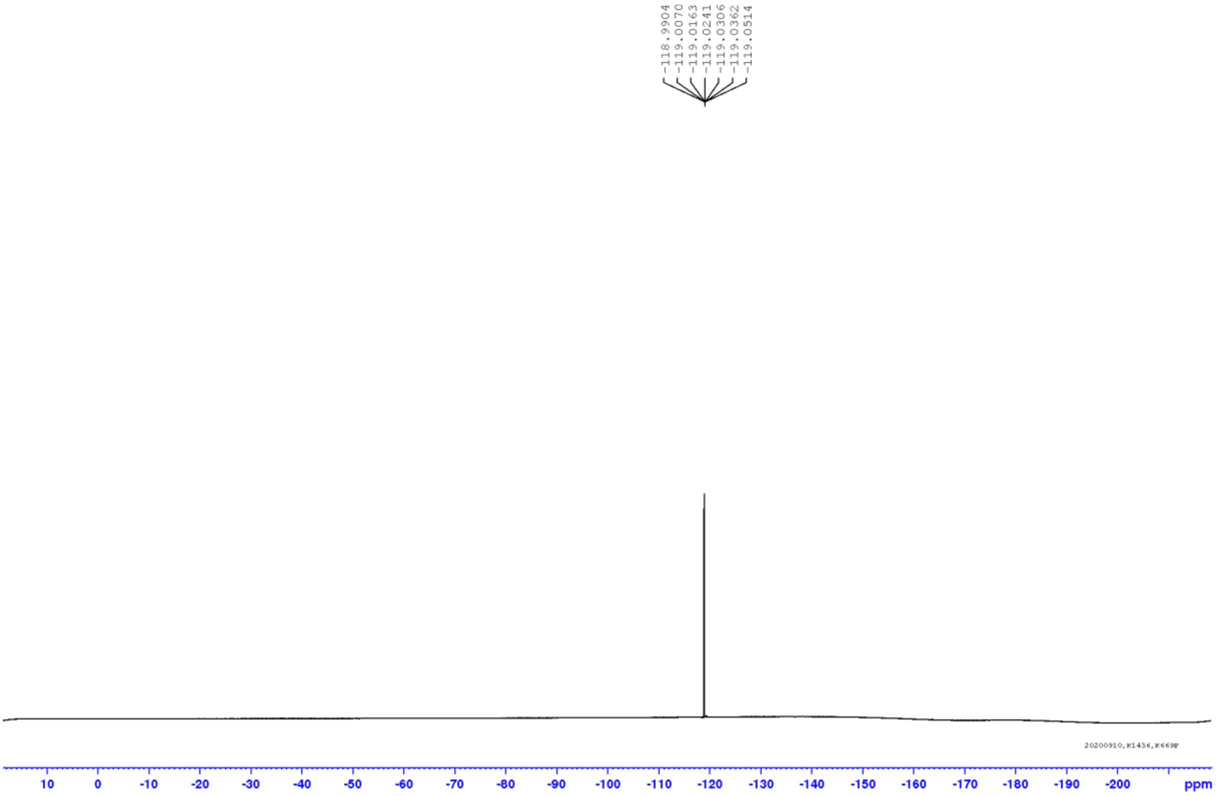

1,2-Bis(3,5-bis(trifluoromethyl)phenyl)ethane

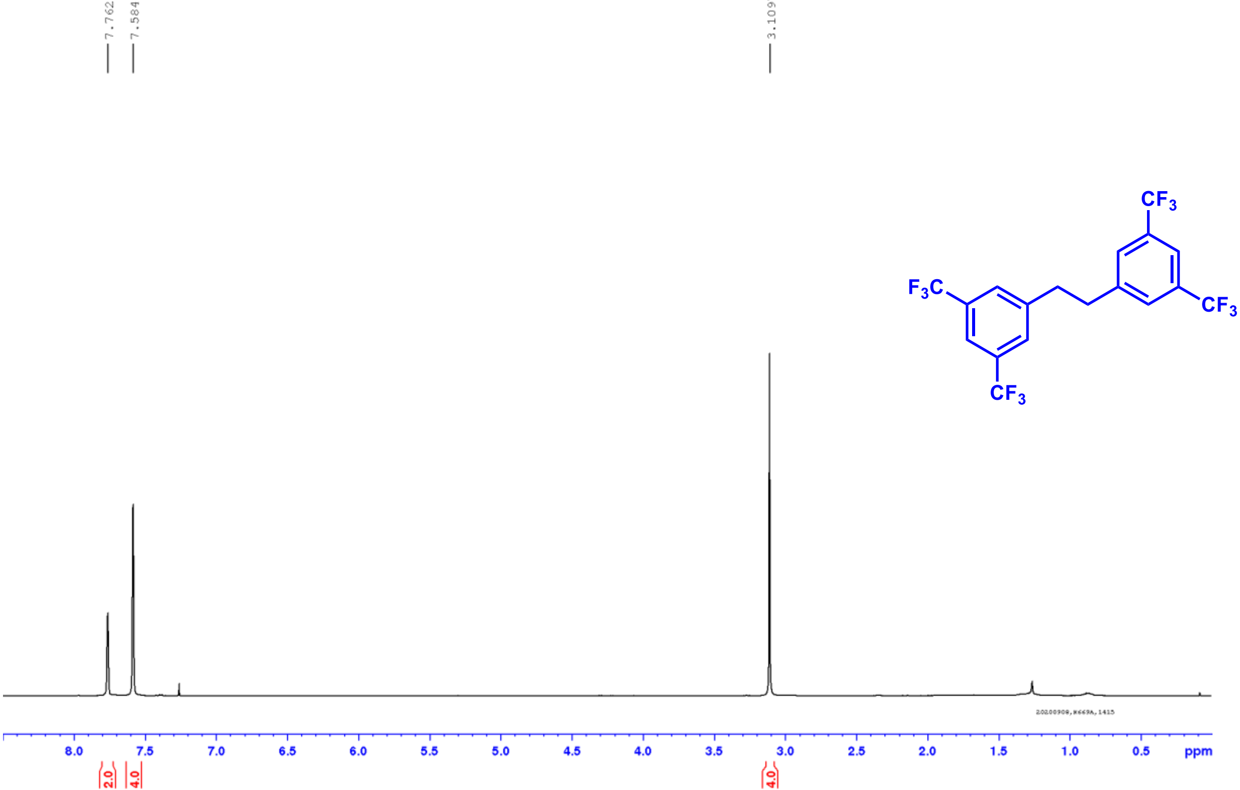

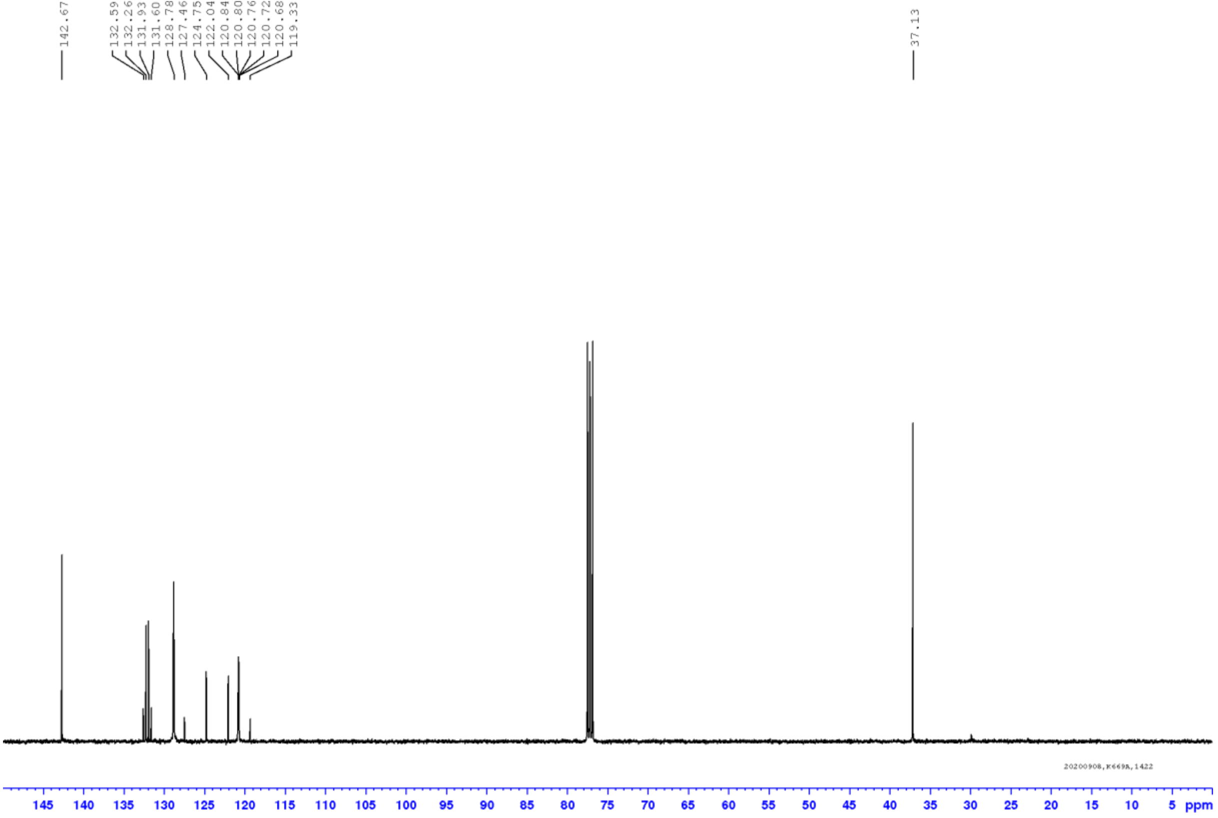

1,2-Bis(3,5-bis(trifluoromethyl)phenyl)ethane

^{19}F NMR

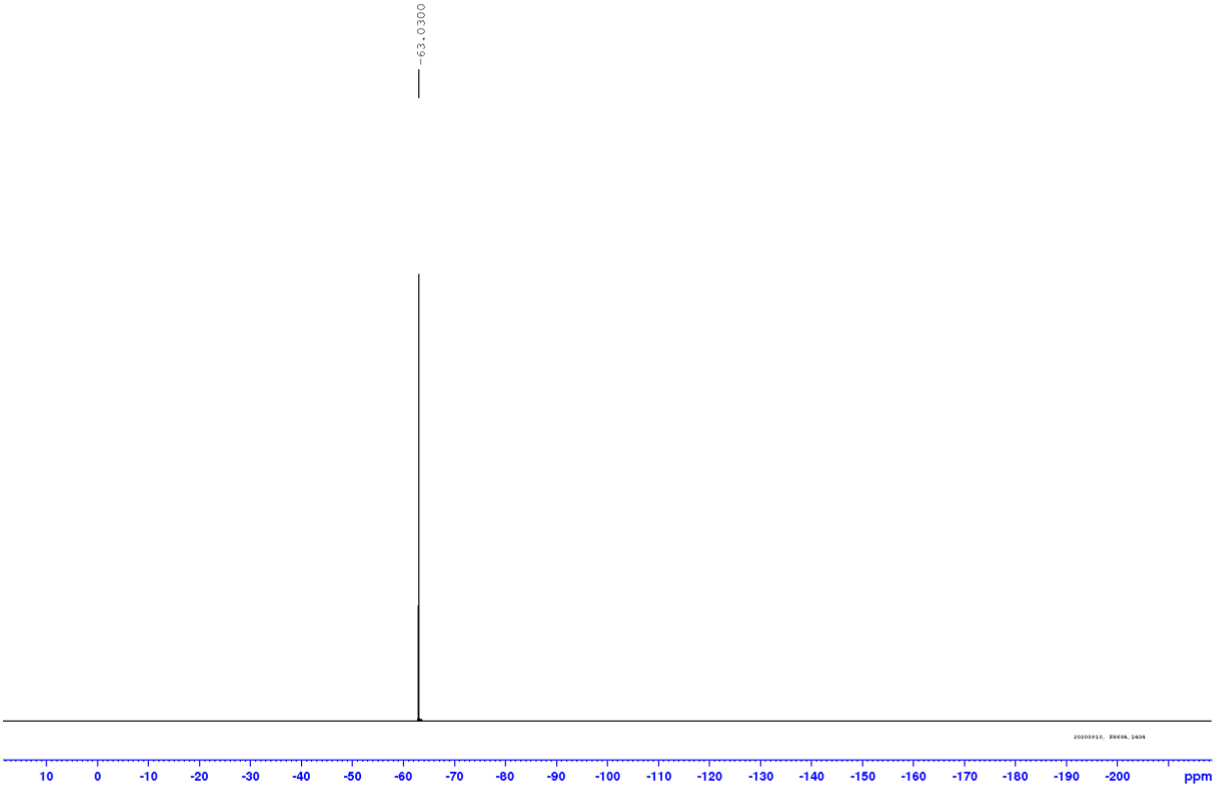

1,2-Bis(perfluorophenyl)ethane

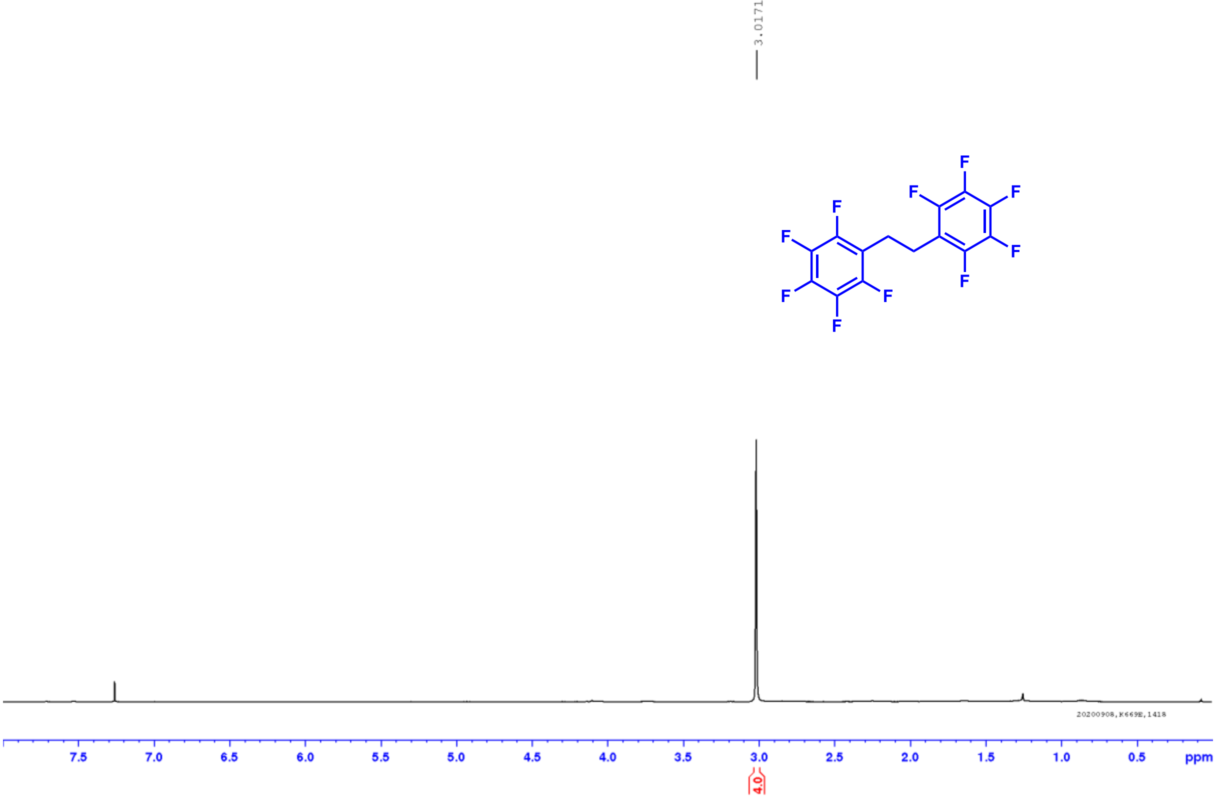

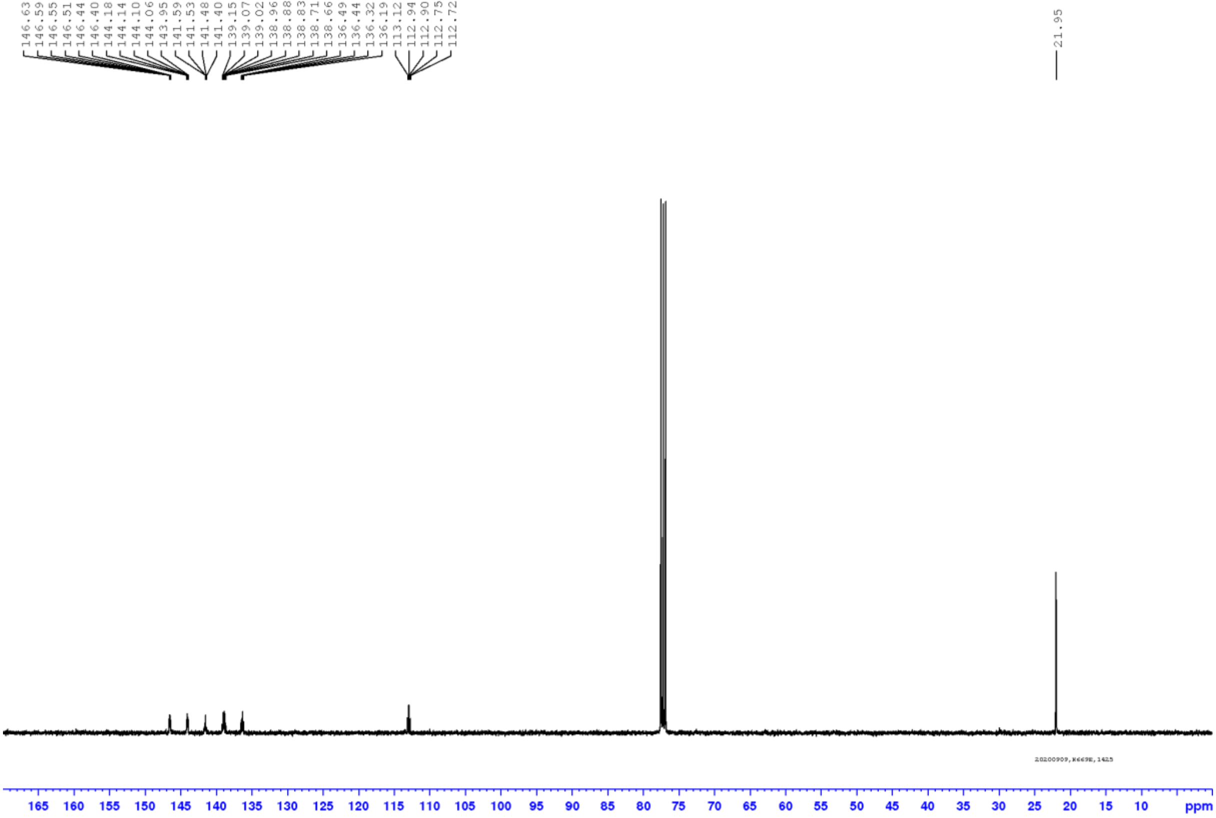

1,2-Bis(perfluorophenyl)ethane

^{19}F NMR